Energy harvesting by bio-inspired inverted C-cylinders in stagger arrangements

Author

Shaban Nawaz

Regn Number

2019-NUST-MSME-317541

Supervisor

Dr. Emad Uddin

DEPARTMENT OF MECHANICAL ENGINEERING

SCHOOL OF MECHANICAL & MANUFACTURING ENGINEERING

NATIONAL UNIVERSITY OF SCIENCES AND TECHNOLOGY

ISLAMABAD

NOVEMBER, 2021

Declaration

I certify that this research work titled "*Energy harvesting by bio-inspired inverted C-cylinders in stagger arrangements*" is my own work. The work has not been presented elsewhere for assessment. The material that has been used from other sources it has been properly acknowledged/referred.

Signature of Student: _____

Shaban Nawaz

2019-NUST-MSME-317541

Copyright Statement

Acknowledgements

I am thankful to my Creator Allah Subhana-Watala to have guided me throughout this work at every step and for every new thought which You setup in my mind to improve it. Indeed, I could have done nothing without Your priceless help and guidance. Whosoever helped me throughout the course of my thesis, whether my parents or any other individual was Your will, so indeed none be worthy of praise but You.

I am profusely thankful to my beloved parents who raised me when I was not capable of walking and continued to support me throughout in every department of my life.

I would also like to express special thanks to my supervisor Dr. Emad Uddin for his help throughout my thesis. Each time I got stuck in something, he came up with the solution. Without his help I wouldn't have been able to complete my thesis. I appreciate his patience and guidance throughout the whole thesis.

I would also like to thank Dr. Zaib Ali, Dr. Muhammad Sajid and Dr. Niaz Bahadur Khan for being on my thesis guidance and evaluation committee and express my special thanks to Dr. Usman Latif for his help.

Finally, I would like to express my gratitude to all the individuals who have rendered valuable assistance to my study.

Dedicated to my exceptional parents and adored siblings whose tremendous support and cooperation led me to this wonderful accomplishment

Abstract

To use the well-adapted models and structures of living organisms for solving engineering problems is known as biomimetics. As the piezoelectric eel is placed in the wake of a bluff body, the strain is developed in the eel and the electrical voltage is generated which is sufficient to provide the power to sensors in the ocean. The bio-inspired fins like dorsal, pectoral and pelvic affixed on the 120°, 150°, and 180° cut angle inverted C-cylinders are used as a bluff body, and the investigation in terms of electrical voltage, flapping frequency, and peak-to-peak oscillating amplitude is done. These parameters are examined by varying Gx (ratio of horizontal distance between the center of the cylinder and the leading edge of eel by the diameter of a cylinder) from 1 to 2.5 and Gy from 0.5 to 1.5. Maximum energy is harvested when a flag is near the point of high amplitude and frequency causing more deformation and strain rate. The maximum power of 84.88 μW is noticed when the dorsal fin affixed on 180° cut angle cylinder is used as a bluff body. The trailing edge of the eel covers the maximum amplitude of 14.818 mm, 5.45 cycles per second for the case of Gx=2 and Gy=0.5. The percentage increment of 39.68 is noticed by using Dorsal 180° rather than pectoral 180° cut angle cylinder.

Keywords

Piezoelectric eel, bluff body, bio-inspired inverted C-cylinders, Energy harvesting, Biomimetics

Table of Contents

List of Figures

List of Tables

Chapter 1

Introduction

1.1 Biomimetics

Living organisms have well-adapted models and structures that's why researchers use these to solve their engineering problems which is known as biomimetics. A lot of research is being done on oceans which needs many types of sensors to collect and evaluate the data regarding environmental issues, marine life, pollution, and disasters, etc [1]. To provide the power to those sensors via micro-electromechanical systems (MEMS) is of research interest topic. The reason is that the wireless sensor network can be flexibly installed near the target location due to which it provides more reliable results [2]. The oil and gas departments need many sensors throughout their drilling, extraction, and refining processes to know all the parameters i.e., flow rate, temperature, and pressure, etc. The department prefers wireless sensor networks over a traditional system to get an efficient system with low equipment wear. The temporary installation of sensor in remote areas prefer this type of technology rather than the conventional wired sensor network [3].

1.2 Energy harvesting

Energy can be extracted or used to modify the fluid properties such as pressure, flow rate as a requirement through biomedical devices. The conversion between mechanical and electrical signals can be brought by using many effects such as electromagnetic, electrostatics, electrodynamics, piezoelectric and triboelectric. Due to flexible adjustment and producing high amplitude motion for high-frequency flapping, the PVDF flag is mostly used as an energy harvester. Many tissues of the body i.e., tendon, cartilage, ligaments even bone are piezoelectric materials in nature. [4] , [5].

When a piezoelectric crystal is not under any stress, there is no electrical signal produced by this crystal fixed between two metal plates because the charge is in balance. Bluff body in the path of flowing fluid produces the wakes which cause mechanical stress on the piezoelectric crystal. In

response to mechanical stress, positive and negative charges collect on the metal plates which causes to produce enough electricity to charge the sensors underwater. [6].

1.3 Piezoelectricity

Piezoelectricity is a kind of electricity that results from latent heat and pressure. The piezoelectric effect is the tendency of certain materials to generate electrical energy when mechanical stress or pressure acts on them. The same materials have tendency to produce mechanical stress when electrical energy is provided to them [7]. When mechanical pressure is applied to these materials, the centers of positive and negative charges shift which results in the creation of an external electric field. During the inverse piezoelectric effect, an external electric field elongates or compresses the material which develops the mechanical stress or pressure [8]. There are natural and manmade piezoelectric materials available. The manmade piezoelectric materials are of the following categories, polymers, composites, ceramics, thin films, and quarts. The Polyvinylidene difluoride, PVDF is a polymer type of piezoelectric material which is used in this study. Vortex-induced vibration is a source of energy extraction of high interest for research purposes these days [9]. When there is not any object placed in the flowing path of fluid, it will flow in streamlines and there is no vortex. When the body is placed in the flowing path of a fluid, it'll create the vortices from which the energy can be harvested by using a piezoelectric eel.

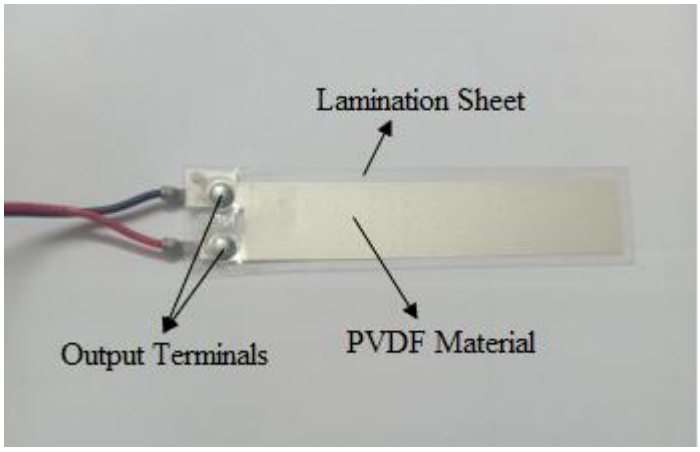

Figure 1.1 Piezoelectric Eel

When the circular cylinder is used as a bluff body, the wake is formed in which the maximum pressure is obtained at the stagnation point. The pressure decreases along the first half of the

cylinder gradually and then it tends to increase along the next half of the cylinder. The flow particles experience the adverse pressure gradient due to which the flow separates from the surface of a bluff body and a highly turbulent region forms which is known as the wake. This separated boundary layer creates a shear layer that rolls into a specific shape and detaches from the surface which is known as vortex shedding. Its rolling pattern depends upon the size and shape of the bluff body and the Reynolds number of flow [10]. These shear layers shed alternatively and produce a vortex pattern in the wake region which is known as the Karaman vortex street [11]. When the vortices are shed, the pressure distribution occurs which causes the vibration known as vortex-induced vibration [12].

1.4 Background

Previous experimental and numerical studies have proved that this harvested power directly depends upon the frequency and flapping area. To optimize this power is a tremendous topic. In the case of the bluff body, the drag is dominated by pressure drag while in the case of streamlines, it is dominated by viscous drag. The flow is dominated by which drag is completely dependent on the shape of the body kept in the flowing path of a fluid. The airfoil at a small attack angle acts as a streamlined body and at a large attack angle, it acts like a bluff body [13]. The brick or any shape of the cylinder causes the pressure drag due to which a separation region occurs that's why there are many kinds of the bluff body when these are kept in the flowing path. The size of the wake is mainly dependent on this separation region and due to eddy formation, the pressure is decreased. This decrement in pressure causes the pressure drag. When the airfoil at a higher angle of attack is used as a bluff body, the flow over its top surface is separated and the pressure drag becomes very high than the viscous drag [14], [15]. At a very low Reynolds number, no separation region occurs and it's a creeping flow. With the increase of Reynolds number, the vortex street changes from laminar to turbulent, and then from laminar separation layer to turbulent on a further increment of Reynolds number (lower transition regime). From supercritical to Transcritical flow regime, the boundary layer becomes fully turbulent on both sides [16], [17].

Various researches are done by changing the sharpness of a bluff body and the effect of flow regime on the harvested energy. The change in flapping frequency and amplitude is studied by using a numerical and experimental approach. It's necessary to study the dimensionless parameters

so that these results might be applicable in real-time world problems. For that, the distance between the center of the bluff body and the leading edge of the eel (S) is divided by the diameter of the cylinder (D). The maximum amplitude is divided by the length of the eel to make it dimensionless amplitude. By doing so, the prototype results would be useful for real-time applications in oceans, oil and gas departments, etc [18], [19].

1.5 Aim and Objectives

The author aims to develop a competent, simple, and robust energy harvesting source from the inverted C cylinders having a cut angle of 120, 150, and 180 degrees combined with bio-inspired dorsal, pectoral and pelvic fin from the ambient flow. Following objectives are set for this study

- To study the effect of flow parameters on energy harvesting by using piezoelectric eel.
- To design bluff bodies with bio-inspired dorsal, pectoral, and pelvic fin on 120, 150, 180-degree cut angle cylinders.
- To compare the amplitude, frequency, and power for these bluff bodies through experimental analysis.
- To find the more convenient bluff body for energy harvesting.

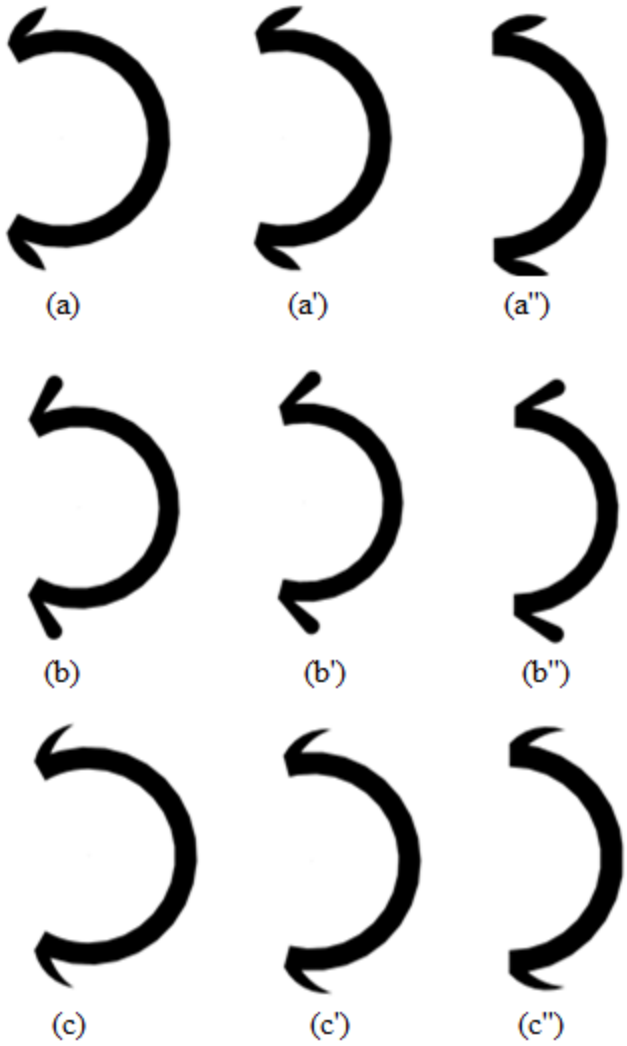

Figure 1.2 Different Cylinders with fins (a) Dorsal 120, (a') Dorsal 150, (a'') Dorsal 180, (b) Pectoral 120, (b') Pectoral 150, (b'') Pectoral 180, (c) Pelvic 120, (c') Pelvic 150, (c'') Pelvic 180

1.6 Thesis Structure

The background and literature review of this research study will be explained in chapter 2. Chapter 3 contains the experimental plan and methodology of how to find out harvested power, flapping frequency, and oscillating amplitude. The experimental data is collected and analyzed, the results are discussed in chapter 4 and what has been concluded is mentioned in chapter 5.

Chapter 2

Literature Review

Bearman et al. [20] studied that when sharp edge bluff bodies are kept in the streamflow of the fluid, at the salient edges the separation angle occurs. The effect of Reynolds number on the separation angle and wake region is studied and concluded that at low Reynolds number the flow is stable. By increasing the Reynolds number, this stability remains but after a specific critical point, it goes to become unstable which mainly affects the harvested power. Zhang et al. [21] have studied the comparison of energy harvesting by using different types of bluff bodies like triangular, circular, D-shape, and square cylinders. It was concluded that wake produced by using square cylinder becomes wider and had a greater area for energy harvesting purposes. The peak average power is increased due to more frequency developed. As the spacing ratio is increased, the vibration frequency becomes higher due to which oscillation amplitude decreases.

2.1 Modified circular cylinder

The solid circular cylinder was attached to a motor and it was given some rotation and then the wake developed by this bluff body is studied by Azadeh-Ranjbar et al. [22]. Due to the large component of cross-flow velocity, the amplitude becomes higher than all the bluff bodies on still. This indicates the higher force acting on the cylinder and this is interlinked with the appearance of high vorticity. Another study of changing the bluff body was studied by Hu et al. [23]. The bluff body in this study was attached with two small rods of different shapes at different positions on a circular cylinder. The upper rods were of the shape of circle, square and equilateral triangle. It was concluded that the attachment of these rods on 45 and 60 degrees cause to harvest more energy. Out of these two cases, the case with 60-degree causes to provide high voltage rather than 45-degree case. Due to the high transverse force coefficient for the bluff body in which small circles are attached on 60-degree causes more frequency and more energy can be harvested than all other cases. The PIV was done to justify the results and to observe the wake region. The same study with y-shaped attachment on the circular cylinder was done by Wang et al. [24].

2.2 Effect of Surface roughness

The energy harvesting and VIV were studied by varying the surface roughness of a circular cylinder by [25], [26], [27], and [28]. By increasing the surface roughness, the amplitude drops more than that of frequency. As a whole, the harvested energy is decreased. The conclusion of these studies predicts that the aging of a cylinder when it is used, causes to increase in the roughness factor on the surface of the bluff body [29], [30] and finally the harvested power goes to decrease with time.

2.3 PTC cylinder

The numerical investigation of the energy harvesting by using the PTC shape, triangular prism shape, quasi-trapezoid shape, and circular cylinders. It was concluded that the energy harvesting for quasi-trapezoid cylinder and PTC cylinder is increased by 45.7% and 37.9% respectively than others. Energy harvesting by using a simple circular cylinder was investigated by using an arc-shaped piezoelectric flag [31] and a T-shaped piezoelectric flag [32].

Flowing fluid generates energy in the form of vortices which can be harvested by using piezoelectric eel [33]. The vortex induces the vibration which can be applied to the eel in the form of pressure. This causes the strain which can be harvested into electrical energy. The change in flapping frequency and the non-dimensional amplitude is studied by [34]. Energy harvesting is studied by using a rectangular plate as a bluff body [35]. This study concludes that the harvested energy is proportional to the dimension of sheet, vorticity, amplitude, and frequency. In the wake of a rectangular bluff body, an array of membranes of piezoelectric eel is used to study their effect on one another by [36]. These researches provide us the direction for further research to improve the efficiency of this robust system. Taylor et al. [37] investigated the effect of fluid velocity on the energy harvested in the water tunnel. The result is that the harvested energy is directly proportional to the cube of the velocity of that fluid up to some extent of velocity.

2.4 Inverted C-cylinder

Beal et al. [38] studies that to put eel after a circular cylinder in the flow of a fluid is a beneficial way to extract the energy rather than by using the square cylinders. A lot of researches [39], [40]

has been done to study the effect of tandem type of arrangement on energy harvesting. The behavior of wake interaction, modes of constructive and destructive was also studied.

Although the above-discussed researches are different from the current study but these are discussed here to show that the shape of the bluff body mainly affects the harvested energy. Harvesting energy by using inverted C-shape cylinders as a bluff body is done which is now enhanced by using the different types of fins on these cut angle cylinders.

Chapter 3

Methodology

The experimental work is performed in a water tunnel provided in the Department of Mechanical Engineering, SMME, NUST Pakistan. The experimental setup is a combined set of water tunnel, Centrifugal pump, Honeycomb structure, Variable frequency driver for motor, Camera, Piezoelectric flag, Bluff body, Source light, DAQ card, Laser, and laser modulator. The water tunnel is a low-speed closed flow setup. The water is circulated through a tunnel via a centrifugal pump whose velocity can be varied from rest to 0.5 m/s which is controlled by a variable frequency drive knob whose frequency can be varied from 0 to 50 Hz.

3.1 Experimental Parameters

The frequency is set to 20 Hz and the velocity of the fluid in this study is 0.31 m/s. The Reynolds number in this research study is

$$Re = \frac{\boldsymbol{\rho\, U\, D}}{\boldsymbol{\mu}} = 8681$$

The size of the test section where the vortex is studied is of length, width, and height 2000, 400, and 400 mm respectively. Few honeycombs of aluminum material with length, width, the height of 1.83, 0.5, and 0.025 meters are mounted in the water tunnel before the test section. The purpose of this hexagonal opening honeycomb is to develop a streamlined flow for testing purposes.

	Parameter	Value
Fluid	Velocity	U = 0.31 m/sec
	Reynolds number	8681
	Blockage ratio	6.25
Cylinder	Outer diameter (Included fin)	D’ = 32mm
	Outer diameter (Excluded fin)	D = 25 mm

	Inner diameter	d = 21 mm
	Cut angle	120, 150, 180 degrees
	Fin type	Dorsal, Pectoral, Pelvic
Flag	Material	PVDF
	Size	72 mm x 12 mm x 64 µm
	Membrane thickness	28 µm
	Poisson ratio	0.46
	Young's modulus	1.38 GPa
	Capacitance	1.44 nF
	Density	1.78 kg/m^3
	Voltage range	10 mV – 100 V
	Storage temperature	-40 °C to +70 °C
	Operating temperature	0 °C to +70 °C
Resistor	Optimal resistance	1 MΩ
Clamping Rod	Diameter	4 mm

Table 3.1 Experimental System Parameters

3.2 PVDF energy harvester

The piezoelectric flag (PVDF DT2-052K/L w/rivets) is used to convert the strain/pressure applied on it into the electrical voltage at that instant time. The range of output voltage from this type of flag is from 10 mV to 100V which depends on the load resistance and the stress/pressure applied on it. A clamping frame is attached to the walls of the test section for mounting the bluff body and piezoelectric flag. This flag is attached on a circular rod of diameter 4 mm, free on the trailing edge and clamped on its leading edge. The distance between this flag and the bluff body is adjustable along both the x and y-axis via a clamping mechanism. The total length, active length, width, and thickness of this flag are 72 mm, 62 mm, 12 mm, and 28 µm respectively. The active length is short than the actual length of the flag due to attaching with a rod and almost 10 mm

length is fixed due to epoxy resins and adhesive tape. Dorsal, pectoral and pelvic fins are modeled on a circular cylinder having cut angles of 120, 150, and 180 degrees.

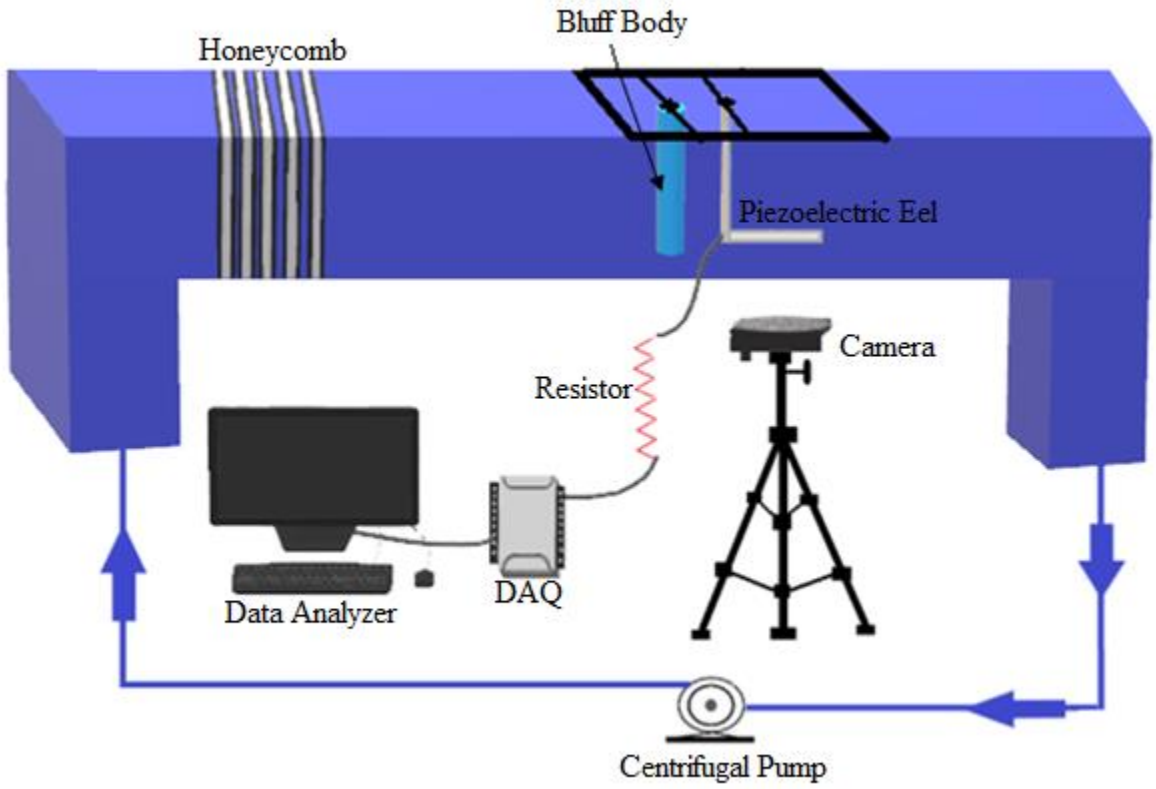

Figure 3.1 Schematic diagram of experimental apparatus

3.3 Data Collection

A Sony RX100 camera is mounted below the test section. The purpose of this high-speed camera is to record the videos of the piezoelectric eel flapping due to the vortex of the bluff body for almost 2 minutes to process this video in MATLAB to find out the flapping amplitude, dimensionless amplitude, and flapping frequency at that specific point from the bluff body. During video recording, to provide better visualization and make the eel prominent, the flashlight is used and the remaining portion is concealed with a thick black cloth. A NI-USB DAQ-6007 card is used as a data acquisition system to record the voltage being produced from the flapping. According to the maximum power transfer theorem, a 1 MΩ resistor is used to provide the load resistance so that the harvested power can be calculated. With a frequency of 50 Hz, the voltage data is gathered

which is read and displayed by LabVIEW software for post-processing. The root mean square value for this gathered data (V_{rms}) is calculated. According to the Ohms law, the harvested power is calculated by using this formula,

$$\boldsymbol{P = \frac{{V_{rms}}^2}{R}}$$

Where P is harvested power, V_{rms} is the RMS value of voltage data taken for almost 120 seconds and R is the optimal resistance which is 1 MΩ according to the maximum power transfer theorem.

$$\boldsymbol{G_x = \frac{X}{D}, \quad G_y = \frac{Y}{D}}$$

Where,

X is the horizontal distance between the leading edge of the eel and the center of the cylinder

Y is the vertical distance between the leading edge of the eel and the center of the cylinder

D is the outer diameter of cylinder excluded fin

D’ is the outer diameter of the cylinder including the fin

d is the inner diameter of the cylinder

A is the maximum amplitude of the piezoelectric flag

L is the length of the piezoelectric flag

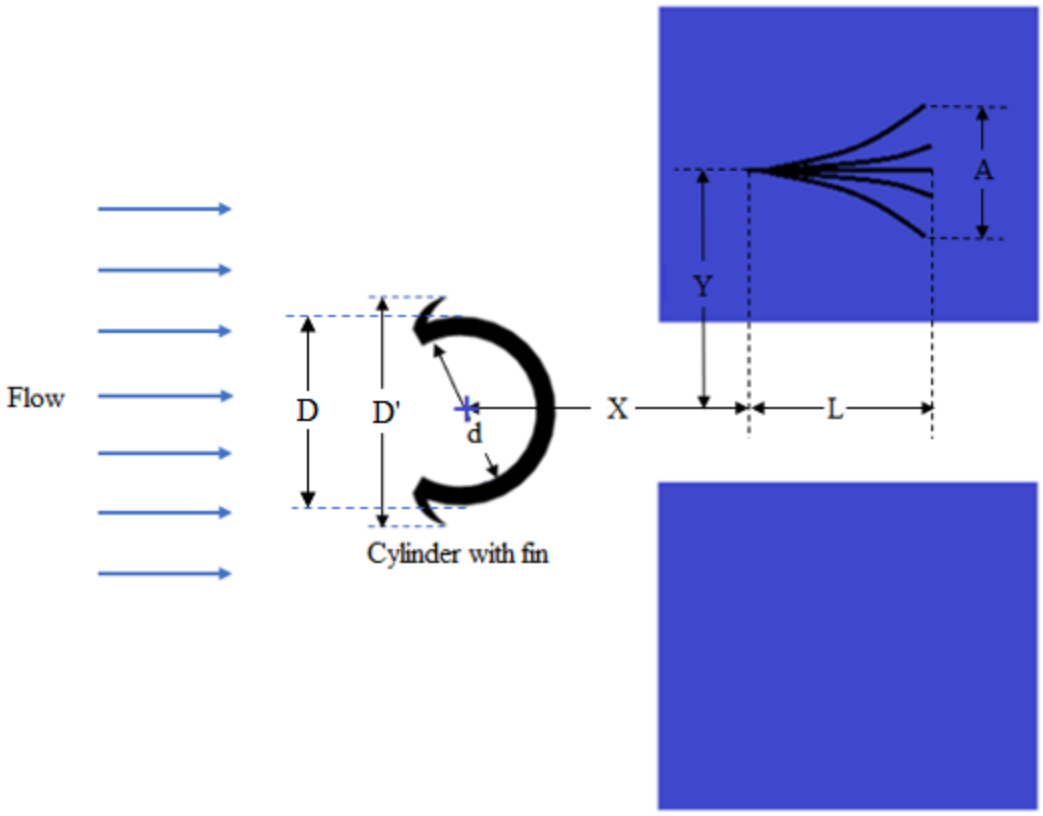

Figure 3.2 Top view of the experimental setup

The MATLAB code is developed by using image processing techniques to point out the tail position of the eel so that by using that data, the amplitude per unit length can be found out. By using the same software, the fast Fourier transformation is used to find out the flapping frequency of the flag by using the recorded video. The comparison of this amplitude per unit length, flapping frequency, and the harvested power is discussed in the next section.

Chapter 4

Results & Discussion

When a piezoelectric flag is placed in the wake of a fluid that is produced due to inserting a bluff body, the strain is developed in the piezoelectric flag. Due to the difference in characteristics of a wave i.e., wavelength, vortices nature, amplitude, and frequency, the developed strain in the eel is also a function of time. This pressure/strain energy is converted into electrical voltage due to the piezoelectric effect. The harvested power is dependent of the strain rate and coupling coefficient, flapping frequency, amplitude, and the parameters of piezoelectric eel [41], [42], [43]. The harvested power is directly dependent upon the cube of flapping frequency and the oscillating amplitude [44]. That's why these two parameters are the key parameters of this study. The results and the comparative study is discussed in these subsections.

4.1 Dorsal fin attached on 120° cut angle cylinder

When the dorsal fin is attached on the 120° cut angle cylinder, and the study area is X from 25 mm to 62.5 mm and Y from 12.5 mm to 37.5 mm. According to the above relations, when these distances are divided by the diameter of the cylinder, Gx becomes from 1 to 2.5 and Gy from 0.5 to 1.5. Figure 5(a) shows the surface plot of harvested power at different points and figure 5(b) shows the flapping frequency and figure 5(c) represents the oscillating amplitude. More frequency is noted near the area where Gy is almost equal to 0.5. As we move away from Gy = 0.5, the frequency tends to decrease. And it tends to decrease as we move away from the '*Max*' point which is represented in figure 5(a) for which Gx is 1.5 and Gy is 0.5. Due to the high speed of deforming in the eel at that point, more power is harvested because it has a direct relation to the cube of strain rate. As we move away from this '*Max*' point, the harvested power is decreased due to the low strain rate. As much as the strain rate is developed in the eel, more voltage is produced according to the direct piezoelectric effect.

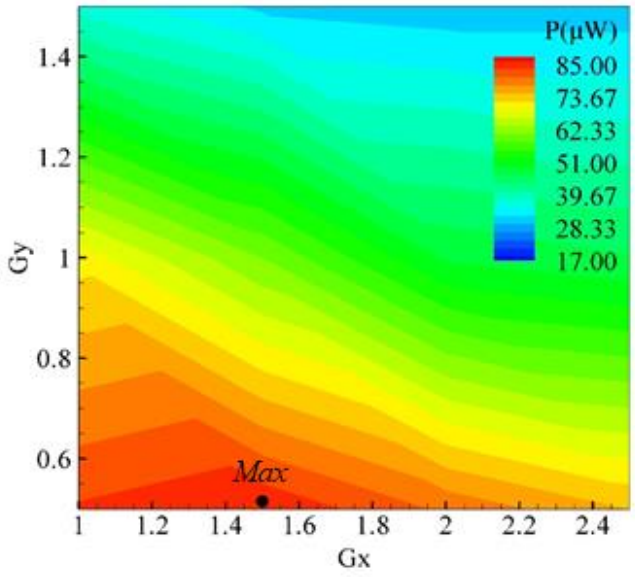

(a)

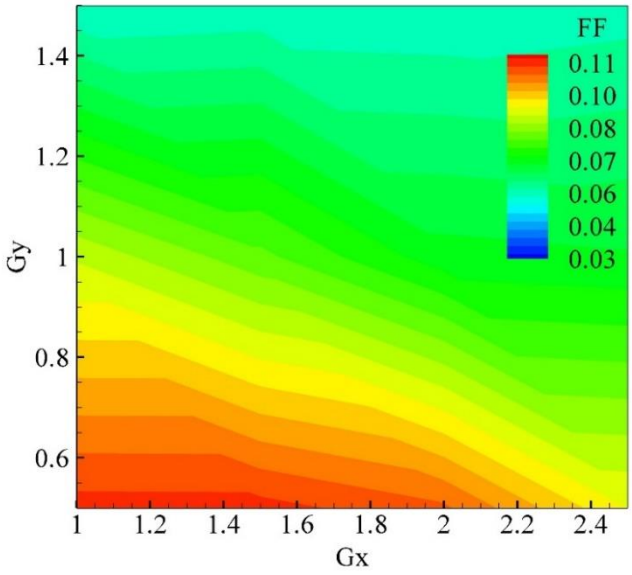

(b)

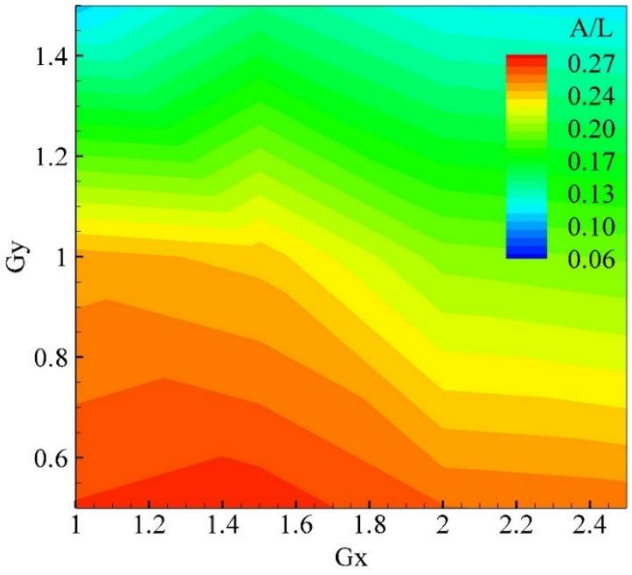

(c)

Figure 4.1 Results by using Dorsal fin attached on 120° cut angle cylinder as a bluff body (a) Harvested power (μW), (b) flapping frequency, and (c) maximum amplitude per unit length.

4.2 Dorsal fin attached on 150° cut angle cylinder

When a dorsal fin is attached to the 150° cut angle cylinder as shown in Figure 2(a') and it is used as a bluff body. All the experimental parameters are the same as in the previous case. The maximum oscillating amplitude in the previous case is 0.267 while in the current case is 0.23. There is no prominent difference in flapping frequency. Due to this loss in amplitude, the covered area by the eel is less which indicates that the applied pressure on the eel is less. When the applied pressure is less, the voltage signal would be low that's why the harvested power is decreased from 84.75 µW to 83.39 µW. The maximum harvested region is near where Gy is almost 0.5 and Gx is from 1.25 to 2.0. As Gy is increased from 0.5, the power tends to decrease due to a lot of decrement in the flapping frequency.

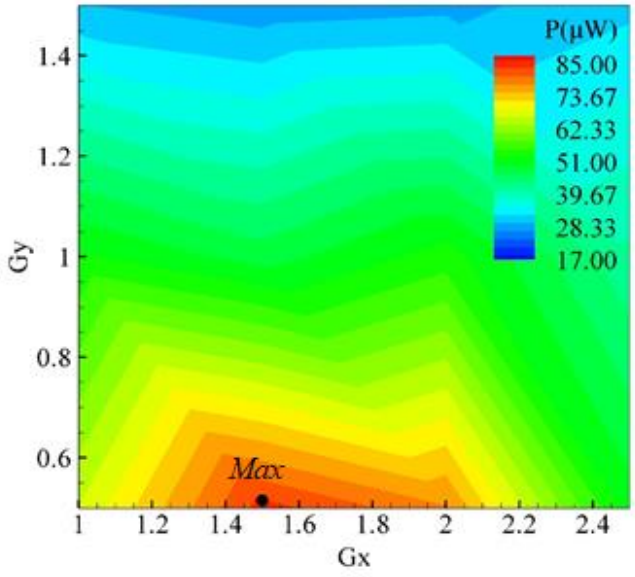

(a)

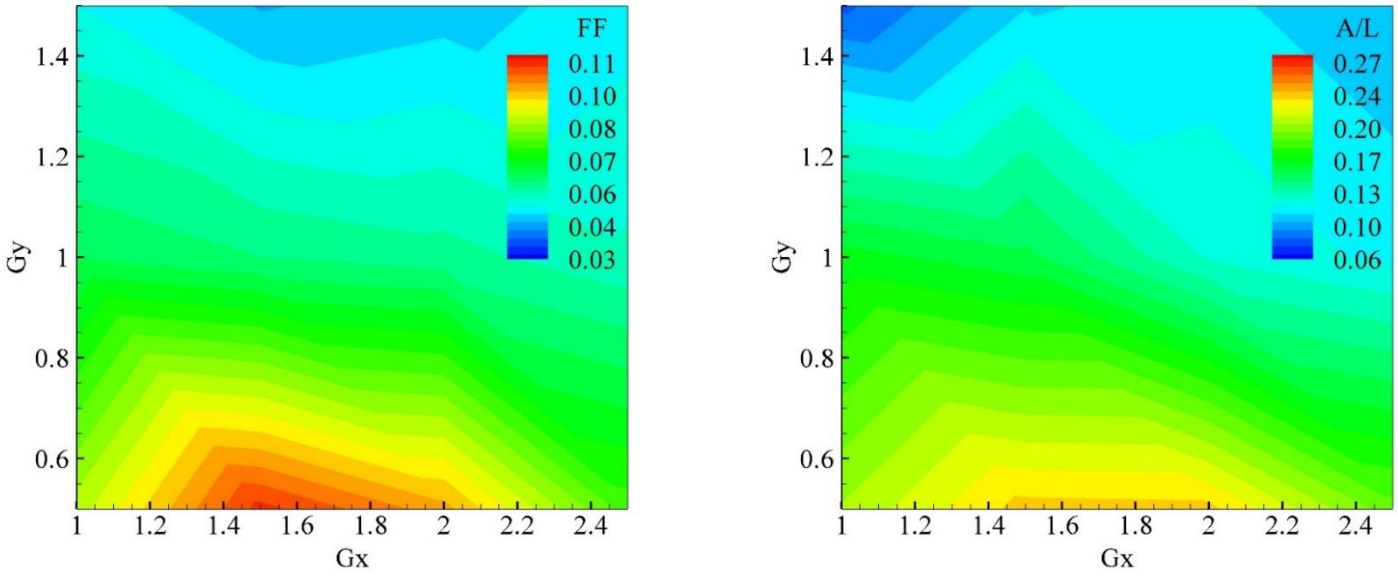

(b) (c)

Figure 4.2 Results by using Dorsal fin attached on 150° cut angle cylinder as a bluff body (a) Harvested power (µW), (b) flapping frequency, and (c) maximum amplitude per unit length.

4.3 Dorsal fin attached on 180° cut angle cylinder

A 180° cut angle cylinder with a dorsal fin is used as a bluff body and all the setup and flow parameters are the same as in the previous cases. The difference in the amplitude is not so notable while the frequency is increased from 0.108 to 0.109 which means that the applied stress on the eel due to the Karman vortices is being applied at a very speed causing the same deformation. The magnitude of deformation in eel is the same but in the current case, it is being very speedily. The data is collected at a frequency of 50 which means that 0.109 x 50 = 5.45 cycles per second. The deformation in eel occurs in such a way that it oscillates 5.45 cycles per second and the total amplitude is 14.818 mm. This optimal point occurs at Gx = 2 and Gy = 0. Due to the more deformation cycles per second, the power of 84.88 µW is harvested which is the 39.68% increment from the minimum case. This scenario is the best out of all other scenarios in this study. Figure 7(d) shows the stroboscopic path of the eel from where we can find the amplitude per unit length which is 14.818 / 62 = 0.239. From figure 7(f), we can notice that the eel covers 27.25 cycles in a timespan of 5 seconds from where we can find out the maximum oscillating frequency of a

piezoelectric eel. The optimal region starts from Gx = 1.2 and tends to increase as we move forward until we reach 2.5. Figure 7(e) indicates the frequency graph for the complete recorded video from where we can find the maximum flapping frequency.

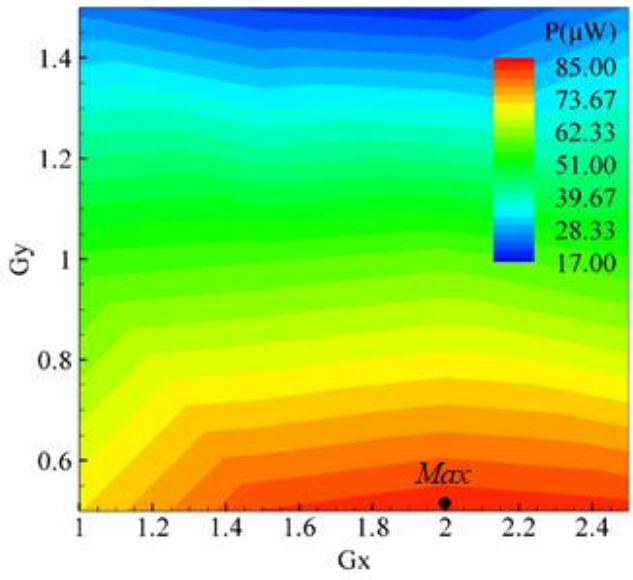

(a)

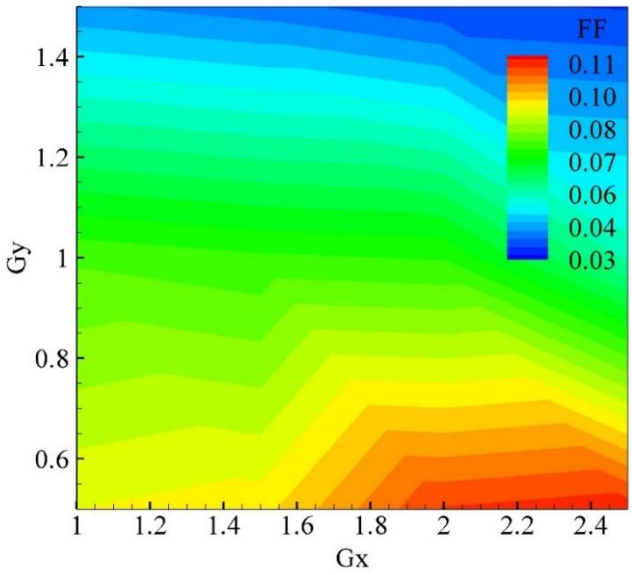

(b)

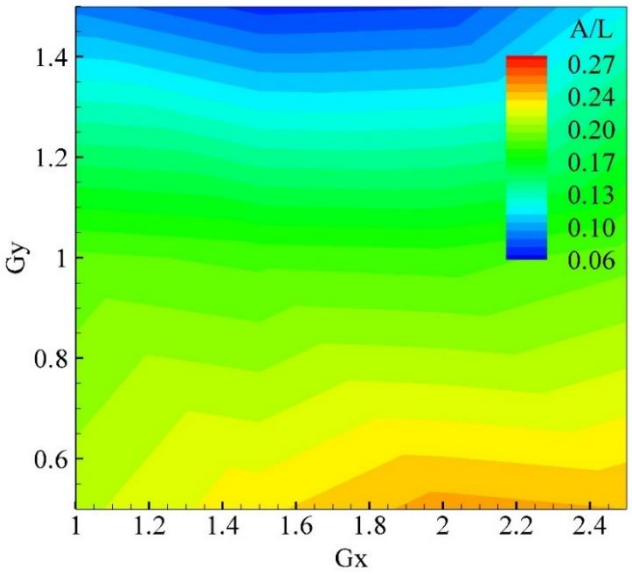

(c)

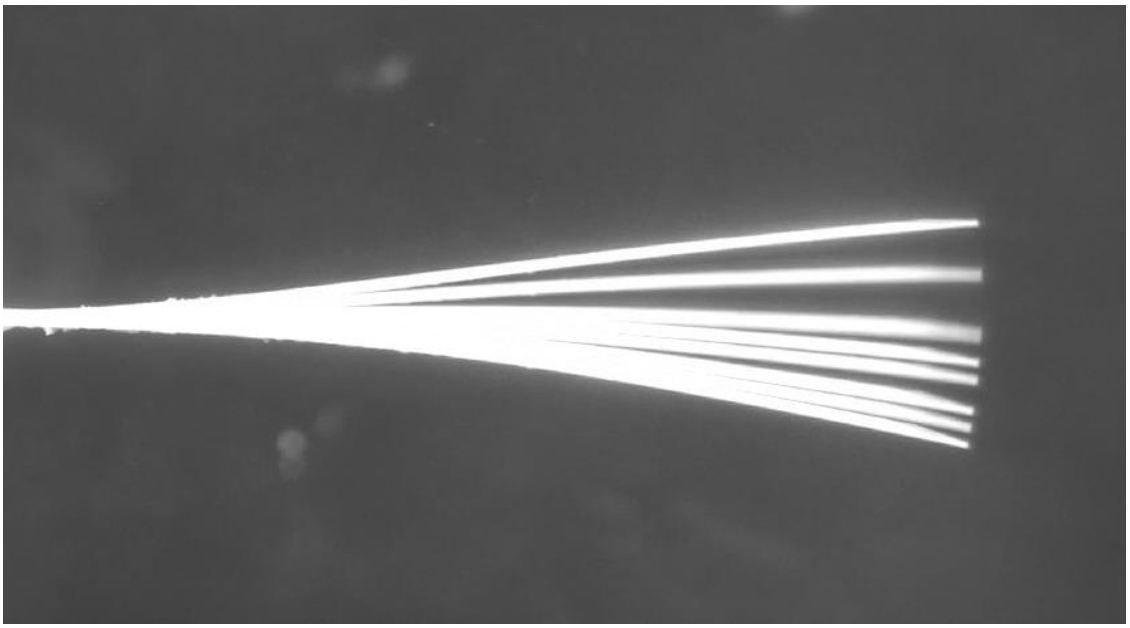

(d)

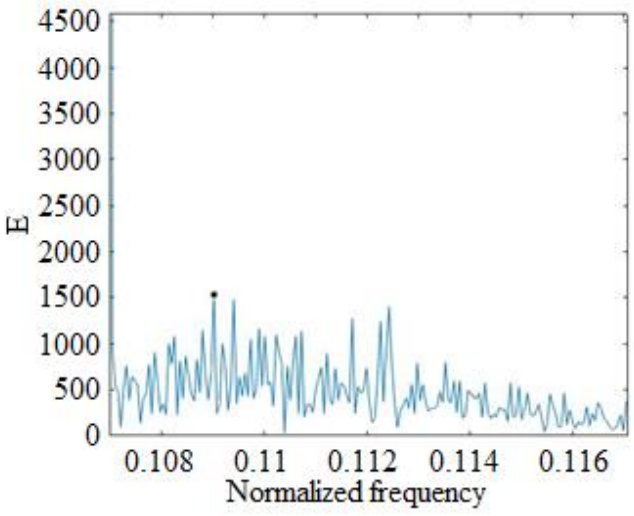

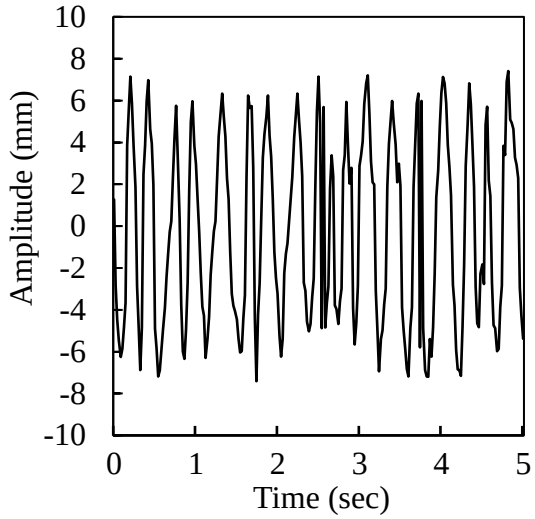

(e) (f)

Figure 4.3 Results by using Dorsal fin attached on 180° cut angle cylinder as a bluff body (a) Harvested power (μW), (b) flapping frequency, (c) maximum amplitude per unit length, (d) stroboscopic behavior of trailing edge of eel, (e) Normalized frequency and (f) Amplitude of trailing edge as a function of time.

4.4 Pectoral fin attached on 120° cut angle cylinder

When a 120° cut angle cylinder along with a pectoral fin is used as a bluff body, the amplitude per unit length decreases from 0.239 to 0.237 which is not so significant. The notable parameter is the frequency in this scenario which decreases from 0.109 to 0.072 which indicates that the deformation rate of eel is less. The harvested power is directly dependent on the cube of flapping frequency [45]. The magnitude of the strain is almost the same but the rate of deformation of eel is less than that of the previous scenario due to which less voltage is produced on the terminals. That's why less power is harvested by using this bluff body. The power in the previous case is 84.88 µW but in the present case, the power of 67.99 µW is harvested which is almost 27.7% less. The optimal point is denoted in figure 8(a) by '*Max*' whose coordinates are Gx = 1 and Gy = 1. As we move far from this point in any direction, the harvested power tends to decrease due to the decrement in the flapping frequency.

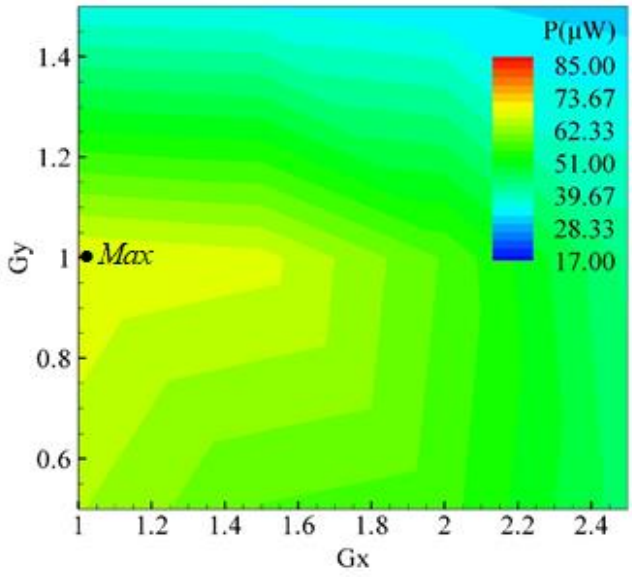

(a)

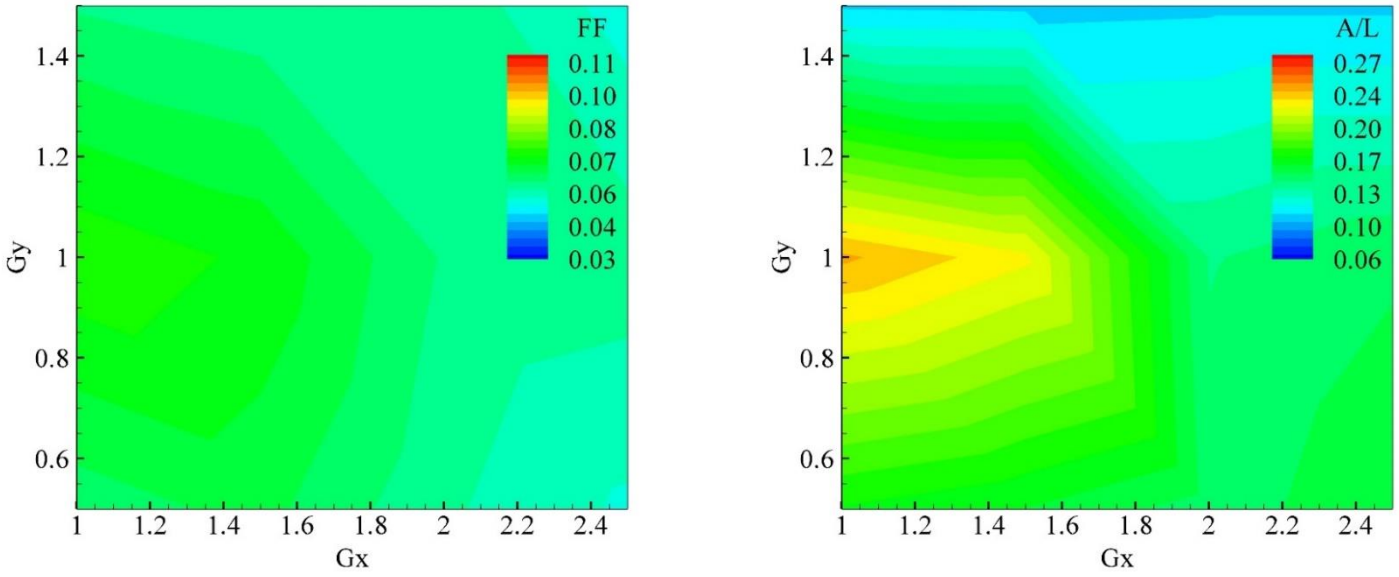

(b) (c)

Figure 4.4 Results by using pectoral fin attached on 120° cut angle cylinder as a bluff body (a) Harvested power (μW), (b) flapping frequency, and (c) maximum amplitude per unit length.

4.5 Pectoral fin attached on 150° cut angle cylinder

When a 150° cut angle cylinder along with a pectoral fin is used as a bluff body, the surface plots of harvested power, flapping frequency, and oscillating amplitude per unit length are shown in figure 9. The effect of the wake produced due to this bluff body and pectoral 120° cut angle cylinder is almost the same in terms of developing strain rate in the eel because it is changed from 0.072 to 0.074 but the magnitude of strain developed is more in this case. This magnitude can be discussed in terms of the amplitude per unit length which is increased from 0.237 to 0.256. As it's understood that the harvested power is directly proportional to the cube of frequency and the amplitude which indicates that the power is mainly dependent on the frequency that on the amplitude. In this scenario, due to the increment in amplitude, the harvested power is increased from 67.99 μW to 69.77 μW. The maximum optimal point is represented by '*Max*' whose coordinates are Gx = 1 and Gy =1 in figure 9(a). As we move from this '*Max*' point, the power tends to less harvest due to the shortage of amplitude. The point having coordinates of Gx = 1.5

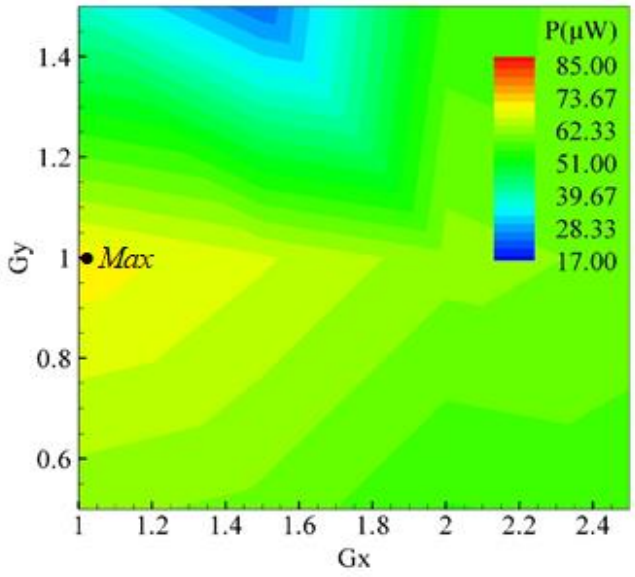

(a)

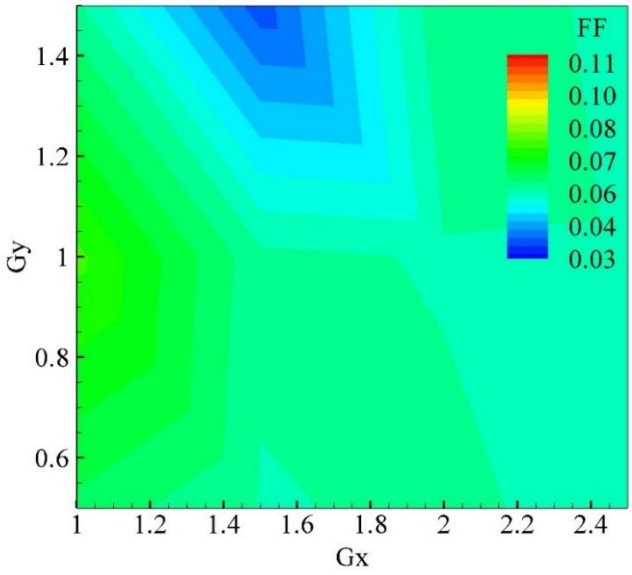

(b)

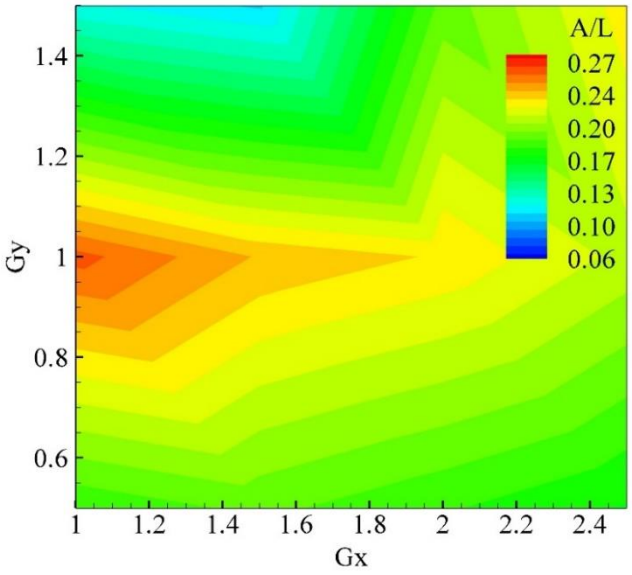

(c)

Figure 4.5 Results by using pectoral fin attached on 150° cut angle cylinder as a bluff body (a) Harvested power (μW), (b) flapping frequency, and (c) maximum amplitude per unit length.

and Gy = 1.5 is noteworthy because this is of the minimum harvested power point in this section. By having a look at the surface graphs, it is concluded that it's less due to the shortage of deformation rate at this point.

4.6 Pectoral fin attached on 180° cut angle cylinder

When a pectoral fin is appended on a 180° cut angle cylinder and is used as a bluff body, the surface plots are shown in figure 10. The magnitude of strain generated and its rate both becomes less in this scenario. The strain generated is represented by the amplitude whose surface plot is in figure 10(c) which indicates that the oscillating amplitude tends to decrease from 0.256 to 0.219 and the strain rate also tends to decrease from 0.074 to 0.064. Due to the low strain developed and low strain rate, fewer charges are collected at the terminals of piezoelectric eel which means that low voltage is generated and harvested power is less which is 60.77 µW. This scenario is an overall very low energy harvesting case in this research study in which very low power is harvested at Gx =1 and Gy = 1 due to very low amplitude at this specific point. Figure 10(d) shows the stroboscopic behavior of the trailing edge of the piezoelectric eel from which we can find the maximum amplitude in mm and then if it is divided by length, it becomes oscillating amplitude per unit length which is 0.219. Figure 10(e) shows the flapping frequency of the complete recorded video from where it can be seen that the peak point where the frequency is 0.064 which means that 0.064 x 50 = 3.2 cycles per second. The piezoelectric eel kept in the wake in this scenario covers 3.2 cycles in each second. Figure 10(f) shows the amplitude of eel for 5 seconds of timespan in which the frequency of cycles and covered area can be noted which is plotted in the surface charts. Figure 10(f) also proves the frequency of 0.064. At the line of Gy = 0.5, the deformation occurs to some extent due to which the harvested power tends to rise to some extent but not more due to not increment in the flapping frequency.

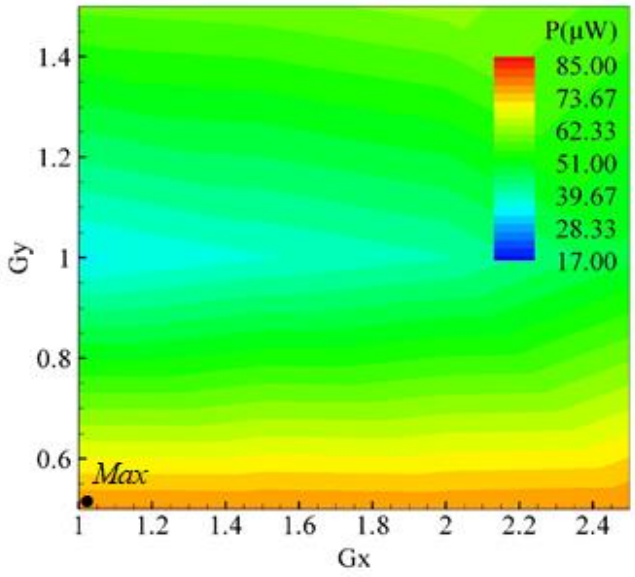
P(μW)
85.00
73.67
62.33
51.00
39.67
28.33
17.00
Max
Gy
Gx
1.4
1.2
1
0.8
0.6
1
1.2
1.4
1.6
1.8
2
2.2
2.4

(a)

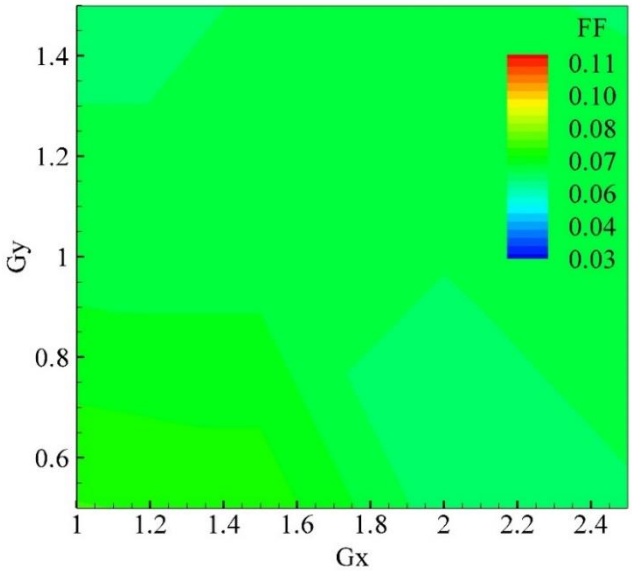
FF
0.11
0.10
0.08
0.07
0.06
0.04
0.03
Gy
Gx
1.4
1.2
1
0.8
0.6
1
1.2
1.4
1.6
1.8
2
2.2
2.4

(b)

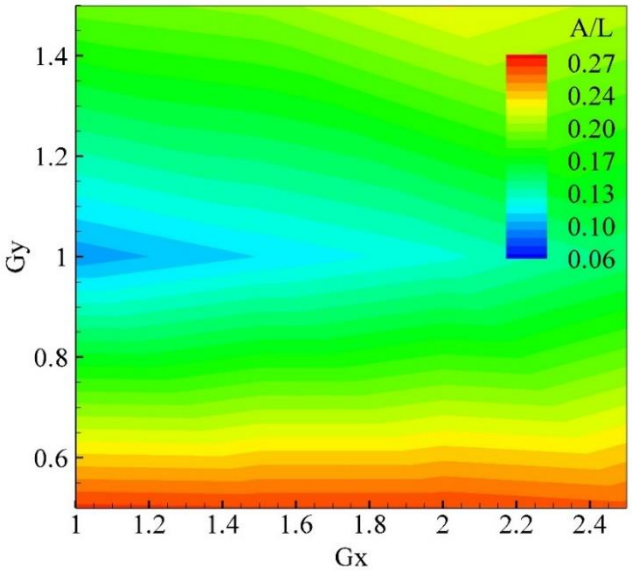
A/L
0.27
0.24
0.20
0.17
0.13
0.10
0.06
Gy
Gx
1.4
1.2
1
0.8
0.6
1
1.2
1.4
1.6
1.8
2
2.2
2.4

(c)

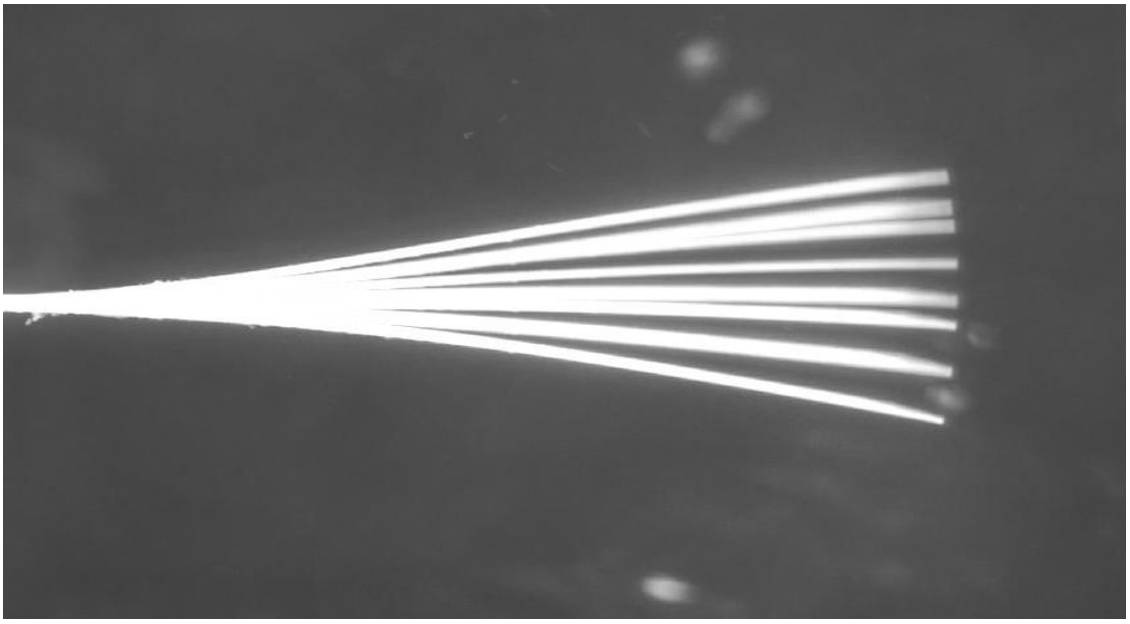

(d)

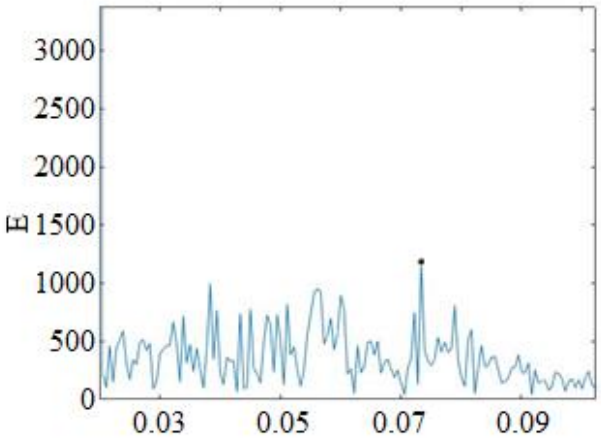

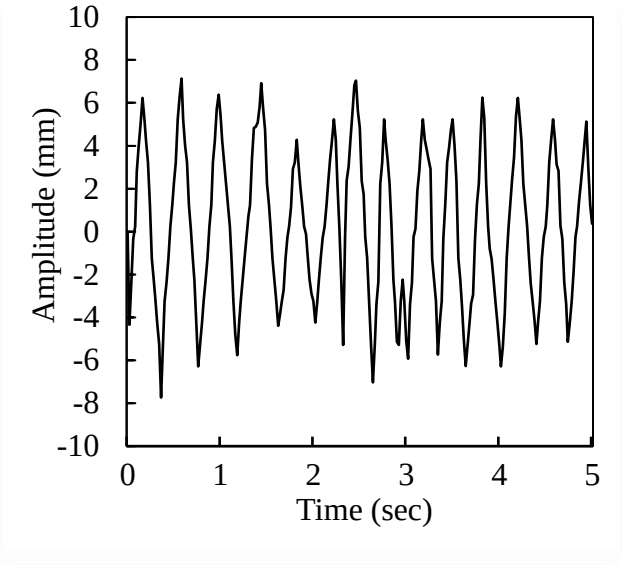

(e) (f)

Figure 4.6 Results by using pectoral fin attached on 180° cut angle cylinder as a bluff body (a) Harvested power (μW), (b) flapping frequency, (c) maximum amplitude per unit length, (d) stroboscopic behavior of trailing edge of eel, (e) Normalized frequency and (f) Amplitude of trailing edge as a function of time.

4.7 Pelvic fin attached on 120° cut angle cylinder

When the pelvic fin affixed on a 120° cut angle cylinder is used as a bluff body, the maximum frequency of 0.108 and peak to peak amplitude of 16.182 mm are noticed. It indicates that by

keeping pelvic 120° cut angle cylinder, maximum amplitude per unit length of 0.261 is noted. The optimal region is covered by Gx from 1 to 1.65 and Gy from 0.5 to 0.65. The optimal point is labeled as '*Max*' in figure 11(a) whose coordinates are Gx = 1.5 and Gy = 0.5. The wake causes more deformation which increased from 0.219 to 0.261 and the strain rate is 0.108 due to which the RMS voltage is increased on the terminals. The maximum power of 83.72 μW is harvested at the '*Max*' point which indicates the 37.78% increase in power.

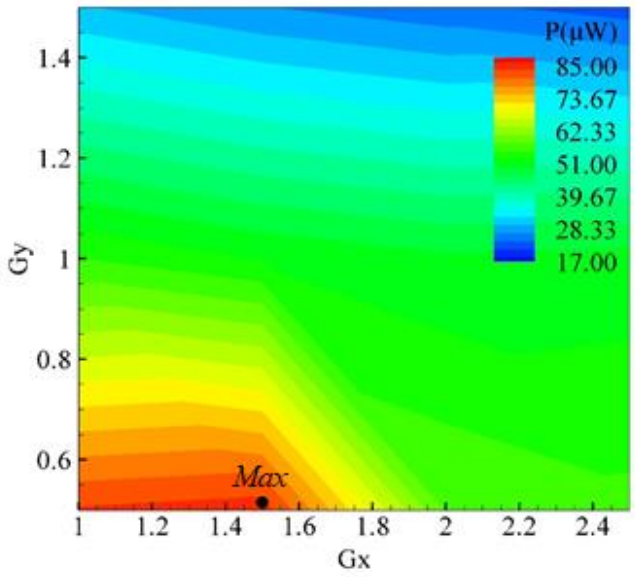

(a)

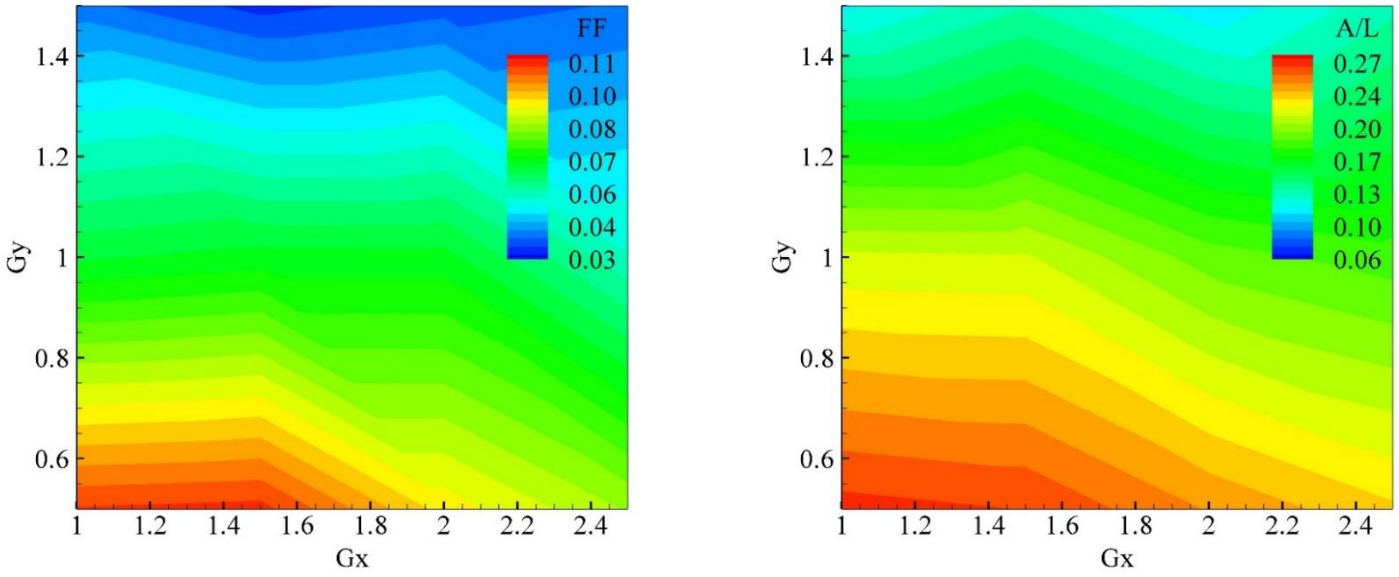

(b) (c)

Figure 4.7 Results by using pelvic fin attached on 120° cut angle cylinder as a bluff body (a) Harvested power (μW), (b) flapping frequency, and (c) maximum amplitude per unit length.

4.8 Pelvic fin attached on 150° cut angle cylinder

When the pelvic fin affixed on 150° cut angle cylinder is kept in the flowing path, the less strain rate is noticed which causes less deformation in the eel. A prominent decrease in flapping frequency is noticed which is from 0.108 to 0.085 which concludes that the eel covers 4.25 cycles in each second. The decrease in the amplitude is also prominent which is from 0.261 to 0.239. Due to decrease in both key parameters, less power is harvested. In this scenario, the maximum power of 71.17 μW is harvested which is a 20.66% decrement from the previous scenario. This optimal point with coordinates of (1.5,0.5) is labeled as Max point in the following figure.

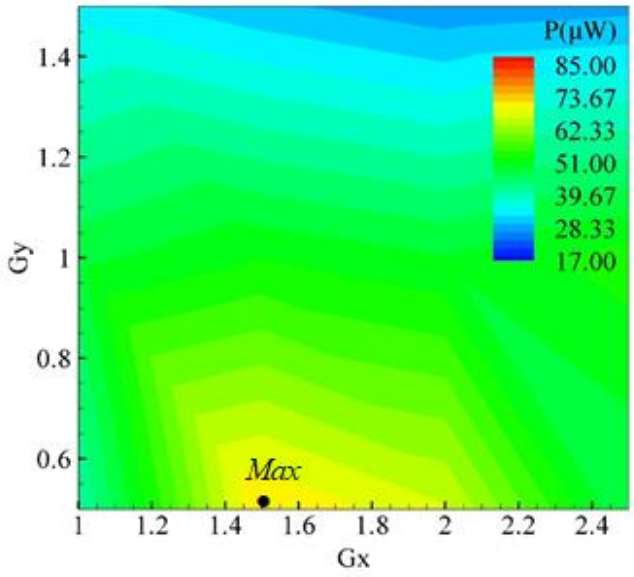

(a)

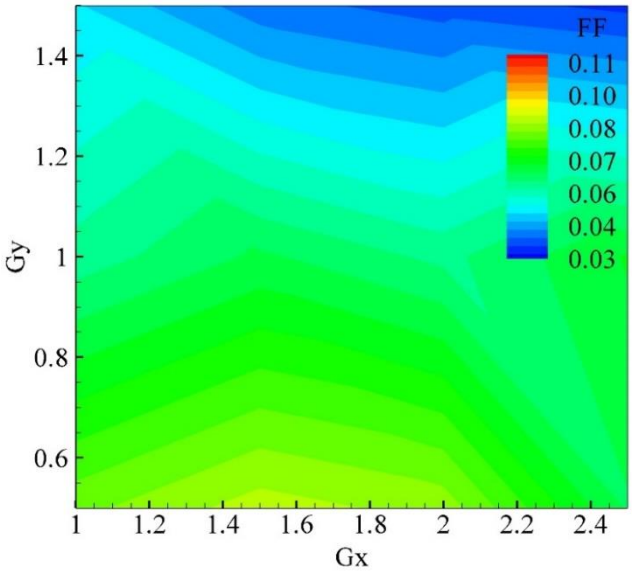

(b)

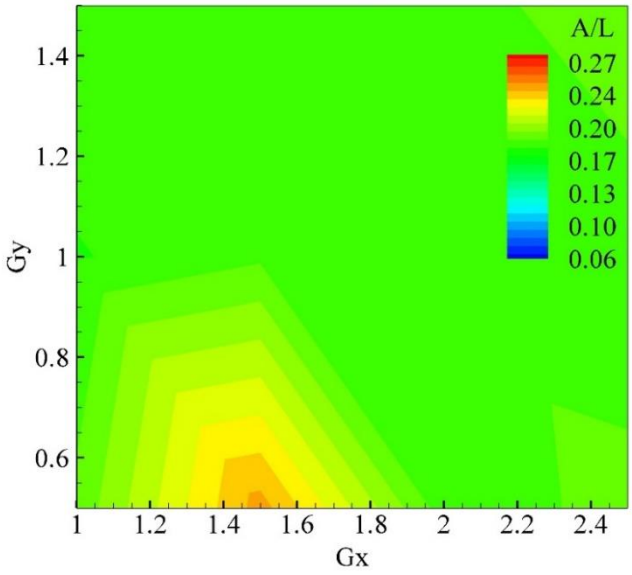

(c)

Figure 4.8 Results by using pelvic fin attached on 150° cut angle cylinder as a bluff body (a) Harvested power (μW), (b) flapping frequency, and (c) maximum amplitude per unit length.

4.9 Pelvic fin attached on 180° cut angle cylinder

The current scenario is similar to that of pelvic 120° cut angle cylinder beside the optimal region

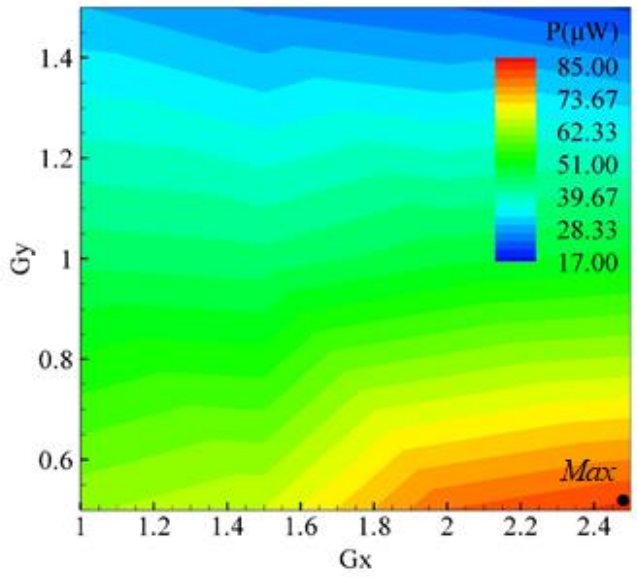

(a)

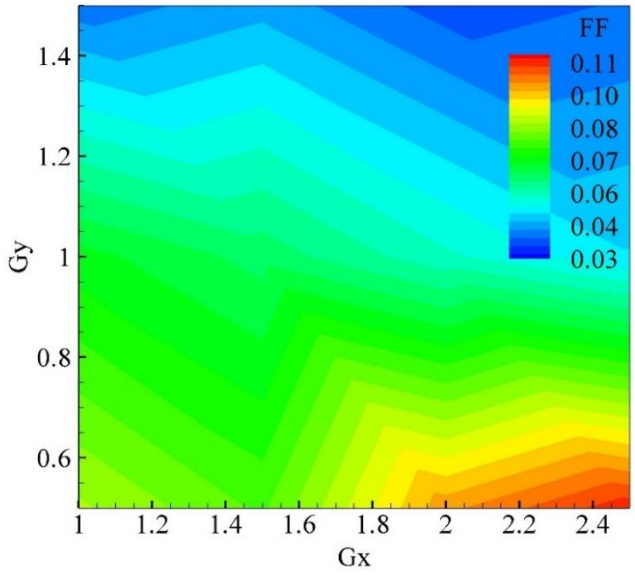

(b)

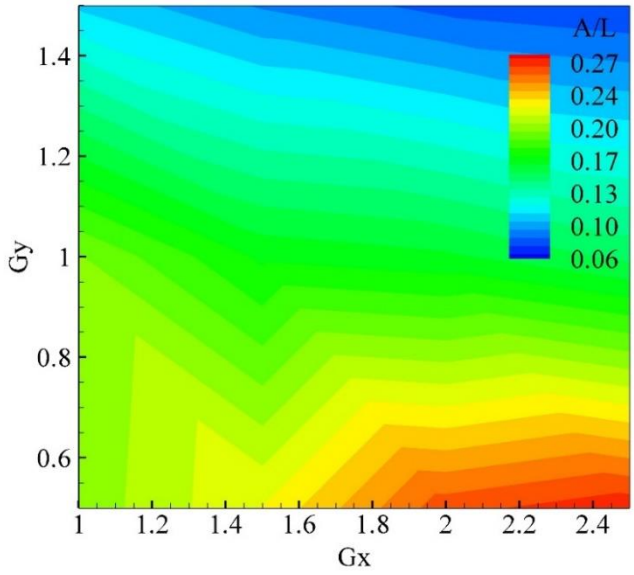

(c)

Figure 4.9 Results by using pelvic fin attached on 180° cut angle cylinder as a bluff body (a) Harvested power (μW), (b) flapping frequency and (c) maximum amplitude per unit length.

which covers Gx from 1.9 to 2.5 on Gy=0.5. The optimal point is at (2.5,0.5) where harvested power is 83.35 µW, the amplitude is 16.62 mm, and the trailing edge of eel covers 5.45 cycles/sec.

4.10 Overall Annotation

Fin Type	Cut Angle	Gx	Gy	P(µW)	FF	A/L	Percentage Increment in Power
Dorsal	120°	1.5	0.5	84.75	0.108	0.267	39.46
	150°	1.5	0.5	83.39	0.108	0.230	37.24
	180°	2.0	0.5	84.88	0.109	0.239	39.68
Pectoral	120°	1.0	1.0	67.99	0.072	0.237	11.89
	150°	1.0	1.0	69.77	0.074	0.256	14.81
	180°	2.0	1.5	60.77	0.064	0.219	0.00
Pelvic	120°	1.5	0.5	83.72	0.108	0.261	37.78
	150°	1.5	0.5	71.17	0.085	0.239	17.12
	180°	2.5	0.5	83.35	0.109	0.268	37.16

Table 4.1 Comparison of all the results; harvested power (µW), flapping frequency, and oscillating amplitude per unit length

The optimal points for each scenario are summarized in table 2 in which the Max point is located via Gx and Gy. The harvested power is a minimum of 60.77 µW for pectoral fin affixed on 180° cut angle cylinder and is maximum of 84.88 for dorsal fin affixed on 180° cut angle cylinder where a 39.68% increase is noticed. The peak-to-peak oscillating amplitude per unit length varies from 0.219 to 0.268 and flapping frequency varies from 0.064 to 0.109. From the above table, it is concluded that the harvested power is directly dependent on the cube of flapping frequency and directly the oscillating amplitude. The optimal minimum point is highlighted by blue color and the optimal maximum point is highlighted by the red color in the above table. The percentage increment in harvested power, flapping frequency, and amplitude are found out by taking the lowest point as a reference. The increment in the percentage of all scenarios can be seen in figure 15.

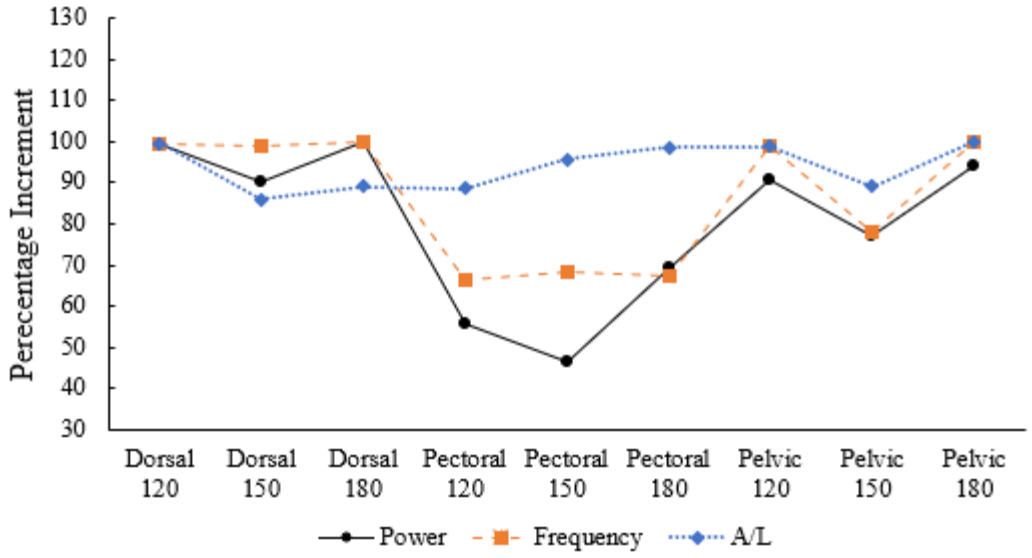

Figure 4.10 Comparison of all the results; harvested power (μW), flapping frequency, and oscillating amplitude per unit length

Chapter 5

Conclusions

In this research study, the energy harvesting by using bio-inspired dorsal, pectoral and pelvic fin affixed on 120°, 150°, and 180° cut angle cylinders is investigated. The area varying Gx from 1 to 2.5 and Gy from 0.5 to 1.5 is studied in terms of RMS voltage, flapping frequency, and peak-to-peak oscillating amplitude. The magnitude and rate of strain developed in the piezoelectric eel directly affect the collection of electrical charges on the terminals of the piezoelectric eel which causes the harvesting of power that's why the maximum power is harvested where the flapping frequency and amplitude is greater. By using a dorsal fin along with a 180° cut angle cylinder as a bluff body, the power of 84.88 μW is harvested which is maximum from all other cases in which the piezoelectric flag covers 5.45 cycles in each second and the trailing edge of eel covers an amplitude of 14.818 mm.

From figure 4.10, it can be concluded that

1. The harvested power from the pectoral fin is the smallest w.r.t all other bluff bodies of this research study. Out of the dorsal and pelvic fin, the dorsal finned bluff bodies are better due to high flapping frequency. According to the harvested power, the fin is arranged as

   Dorsal finned cylinders > Pelvic finned cylinders > Pectoral finned cylinders
2. The harvested power from 150° cut angle finned cylinders is the smallest w.r.t all the bluff bodies of this research study.
3. A lot of change is noticed in frequency which affects the harvested power.
4. Frequency and amplitude both directly affect the harvested power. Out of these two parameters, frequency acts more.
5. Gx = 1.5 and Gy = 0.5 mostly occur as the optimal point for both dorsal and pelvic finned cylinders.

References

[1] I. F. Akyildiz, D. Pompili and T. Melodia, “Underwater acoustic sensor networks: research challenges,” Ad Hoc Networks, vol. 3, no. 3, pp. 257-279, 2005.

[2] Hou, L. and Bergmann, N.W. 2010. System requirements for industrial wireless sensor networks. in Proc. 15th IEEE ETFA, Spain, pp. 1-8.

[3] ON World Inc. ”Oil and Gas Wireless Sensor Networks – A Market Dynamics Report. ”Reasearchandmarkets.com. (accessed February 18, 2019).

[4] Zaszczyńska, A., Gradys, A., & Sajkiewicz, P. (2020). Progress in the Applications of Smart Piezoelectric Materials for Medical Devices. *Polymers*, *12*(11), 2754.

[5] Latif, U., Uddin, E., Abdullah, C., Ali, Z., Sajid, M., Akhtar, K., & Shah, S. R. (2020). Experimental investigation of energy harvesting behind a bluff body. Journal of Renewable and Sustainable Energy, 12(3), 033301. doi:10.1063/1.5144347

[6] Rupitsch, S. J. (2019). Piezoelectricity. In Piezoelectric Sensors and Actuators (pp. 43-81). Springer, Berlin, Heidelberg.

[7] Qiu, C., Wang, B., Zhang, N., Zhang, S., Liu, J., Walker, D., ... & Li, F. (2020). Transparent ferroelectric crystals with ultrahigh piezoelectricity. Nature, 577(7790), 350-354.

[8] Sunil, P., Kumar, S., & Poddar, K. (2020). Wake modification of a forced circular cylinder with an attached filament. Journal of Flow Visualization and Image Processing, 27(3).

[9] Yang, J., Zhang, Y., Chen, H., & Fu, S. (2020). Flow separation control in a conical diffuser with a Karman-vortex generator. Aerospace Science and Technology, 106, 106076.

[10] Kamphuis JW. Hydrodynamics around cylindrical structures. Coast Eng 1998;33:69. https://doi.org/10.1016/S0378-3839(97)00031-8.

[11] Xie, X. D., Wang, Q., & Wu, N. (2014). Energy harvesting from transverse ocean waves by a piezoelectric plate. International Journal of Engineering Science, 81, 41-48.

[12] Viet, N. V., Xie, X. D., Liew, K. M., Banthia, N., & Wang, Q. (2016). Energy harvesting from ocean waves by a floating energy harvester. Energy, 112, 1219-1226.

[13] Wu, N., Wang, Q., & Xie, X. (2015). Ocean wave energy harvesting with a piezoelectric coupled buoy structure. Applied Ocean Research, 50, 110-118.

[14] Mirab, H., Fathi, R., Jahangiri, V., Ettefagh, M. M., & Hassannejad, R. (2015). Energy harvesting from sea waves with consideration of airy and JONSWAP theory and optimization of energy harvester parameters. Journal of Marine Science and Application, 14(4), 440-449.

[15] Xie, X. D., Wang, Q., & Wu, N. (2014). A ring piezoelectric energy harvester excited by magnetic forces. International Journal of Engineering Science, 77, 71-78.

[16] Davidson, J. (2016). Energy harvesting for marine based sensors (Doctoral dissertation, James Cook University).

[17] Tsai, C. W., Shen, S. C., Chang, S. J., Chen, Y. C., & Fang, M. J. (2015, April). A small elastic floating energy harvester for ocean ripple power using knitted PVDF thin film. In 10th IEEE International Conference on Nano/Micro Engineered and Molecular Systems (pp. 461-465). IEEE.

[18] Yoon, S. J., Arakawa, K., & Uchino, M. (2015). Development of an energy harvesting damper using PVDF film. International Journal of Energy Research, 39(11), 1545-1553.

[19] Woo, M. S., Hong, S. K., Jung, H. J., Yang, C. H., Song, D., & Sung, T. H. (2012, July). Strain control for optimization of piezoelectric energy harvesting. In Proceedings of ISAF-ECAPD-PFM 2012 (pp. 1-4). IEEE.

[20] Bearman, P. W. (1984). Vortex shedding from oscillating bluff bodies. Annual review of fluid mechanics, 16(1), 195-222.

[21] Zhang, L. B., Dai, H. L., Abdelkefi, A., & Wang, L. (2019). Experimental investigation of aerodynamic energy harvester with different interference cylinder cross-sections. Energy, 167, 970-981.

[22] Azadeh-Ranjbar, V., Elvin, N., & Andreopoulos, Y. (2018). Vortex-induced vibration of finite-length circular cylinders with spanwise free-ends: Broadening the lock-in envelope. Physics of Fluids, 30(10), 105104.

[23] Hu, G., Tse, K. T., Wei, M., Naseer, R., Abdelkefi, A., & Kwok, K. C. S. (2018). Experimental investigation on the efficiency of circular cylinder-based wind energy harvester with different rod-shaped attachments. Applied energy, 226, 682-689.

[24] Wang, J., Zhou, S., Zhang, Z., & Yurchenko, D. (2019). High-performance piezoelectric wind energy harvester with Y-shaped attachments. Energy conversion and management, 181, 645-652.

[25] Gao, Y., Zong, Z., Zou, L., & Jiang, Z. (2018). Effect of surface roughness on vortex-induced vibration response of a circular cylinder. Ships and Offshore Structures, 13(1), 28-42.

[26] Bai, P., Zhou, L., & Du, X. (2021). Molecular dynamics simulation of the roles of roughness ratio and surface potential energy in explosive boiling. Journal of Molecular Liquids, 335, 116169.

[27] Ghazali, M. K. M., Shaharuddin, N. M. R., Ali, A., Siang, K. H., Nasir, M. N. M., & Talib, M. H. A. (2019). Surface Roughness Effect on Vortex-Induced Vibration Phenomenon in Cross-Flow Direction of a Bluff Body. Journal of Advanced Research in Fluid Mechanics and Thermal Sciences, 64(2), 253-263.

[28] Ramzi, N. A. S., Quen, L. K., Abu, A., Siang, K. H., Othman, N. A., Ken, T. L., & Loon, S. C. (2019). Experimental analysis on vortex-induced vibration of a rigid cylinder with different surface roughness. In IOP Conference Series: Materials Science and Engineering (Vol. 469, No. 1, p. 012003). IOP Publishing.

[29] Ding, L., Zhang, L., Wu, C., Mao, X., & Jiang, D. (2015). Flow induced motion and energy harvesting of bluff bodies with different cross sections. Energy Conversion and Management, 91, 416-426.

[30] Zhang, X., Yang, W., Zuo, M., Tan, H., Fan, H., Mao, Q., & Wan, X. (2018). An arc-shaped piezoelectric bistable vibration energy harvester: Modeling and experiments. Sensors, 18(12), 4472.

[31] Hu, Y., Yang, B., Chen, X., Wang, X., & Liu, J. (2018). Modeling and experimental study of a piezoelectric energy harvester from vortex shedding-induced vibration. Energy conversion and management, 162, 145-158.

[32] Naseer, R., Dai, H. L., Abdelkefi, A., & Wang, L. J. A. E. (2017). Piezomagnetoelastic energy harvesting from vortex-induced vibrations using monostable characteristics. Applied Energy, 203, 142-153.

[33] Allen, J. J., & Smits, A. J. (2001). Energy harvesting eel. Journal of fluids and structures, 15(3-4), 629-640.

[34] Techet, A. H., Allen, J. J., & Smits, A. J. (2002, May). Piezoelectric eels for energy harvesting in the ocean. In The Twelfth International Offshore and Polar Engineering Conference. OnePetro.

[35] Taylor, G. W., Burns, J. R., Kammann, S. M., Powers, W. B., & Welsh, T. R. (2001). SPECIAL ISSUE ON AUTONOMOUS OCEAN-SAMPLING NETWORKS-SPECIAL ISSUE PAPERS-The Energy Harvesting Eel: A Small Subsurface Ocean/River Power Generator. IEEE Journal of Oceanic Engineering, 26(4), 539-547.

[36] Beal, D. N., Hover, F. S., Triantafyllou, M. S., Liao, J. C., & Lauder, G. V. (2006). Passive propulsion in vortex wakes. Journal of Fluid Mechanics, 549, 385-402.

[37] Kim, S., Huang, W. X., & Sung, H. J. (2010). Constructive and destructive interaction modes between two tandem flexible flags in viscous flow. Journal of fluid mechanics, 661, 511-521.

[38] Roeller, K., Blaschke, J., Herminghaus, S., & Vollmer, J. (2014). Arrest of the flow of wet granular matter. Journal of fluid mechanics, 738, 407-422.

[39] Doaré, O., & Michelin, S. (2011). Piezoelectric coupling in energy-harvesting fluttering flexible plates: linear stability analysis and conversion efficiency. Journal of Fluids and Structures, 27(8), 1357-1375.

[40] Michelin, S., & Doaré, O. (2013). Energy harvesting efficiency of piezoelectric flags in axial flows. Journal of Fluid Mechanics, 714, 489-504.

[41] Shoele, K., & Mittal, R. (2016). Energy harvesting by flow-induced flutter in a simple model of an inverted piezoelectric flag. Journal of Fluid Mechanics, 790, 582-606.

[42] Mitcheson, P. D., Yeatman, E. M., Rao, G. K., Holmes, A. S., & Green, T. C. (2008). Energy harvesting from human and machine motion for wireless electronic devices. Proceedings of the IEEE, 96(9), 1457-1486.

[43] Liu, F., Hashim, N. A., Liu, Y., Abed, M. M., & Li, K. (2011). Progress in the production and modification of PVDF membranes. Journal of membrane science, 375(1-2), 1-27.

[44] Zhang, J., Xu, Z., Mai, W., Min, C., Zhou, B., Shan, M., ... & Qian, X. (2013). Improved hydrophilicity, permeability, antifouling and mechanical performance of PVDF composite ultrafiltration membranes tailored by oxidized low-dimensional carbon nanomaterials. Journal of Materials Chemistry A, 1(9), 3101-3111.

[45] Zhang, W., Shi, Z., Zhang, F., Liu, X., Jin, J., & Jiang, L. (2013). Superhydrophobic and superoleophilic PVDF membranes for effective separation of water-in-oil emulsions with high flux. Advanced Materials, 25(14), 2071-2076.

Appendix – A

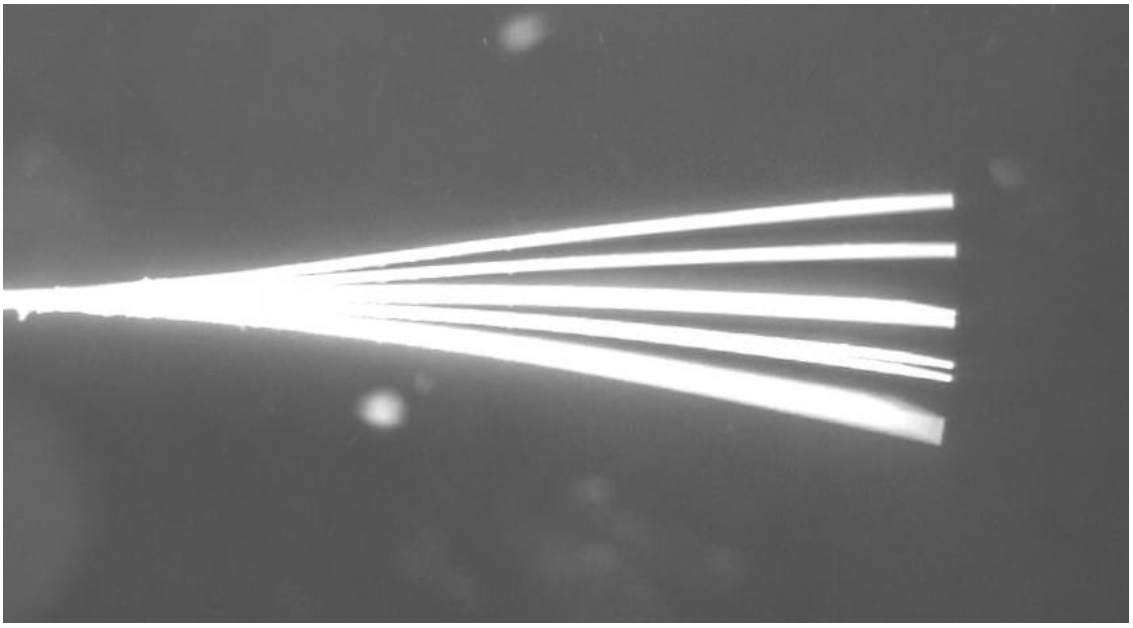

(a)

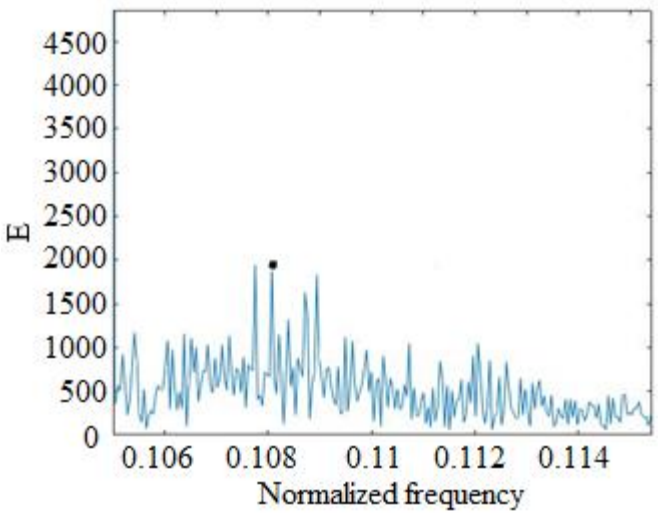

(b)

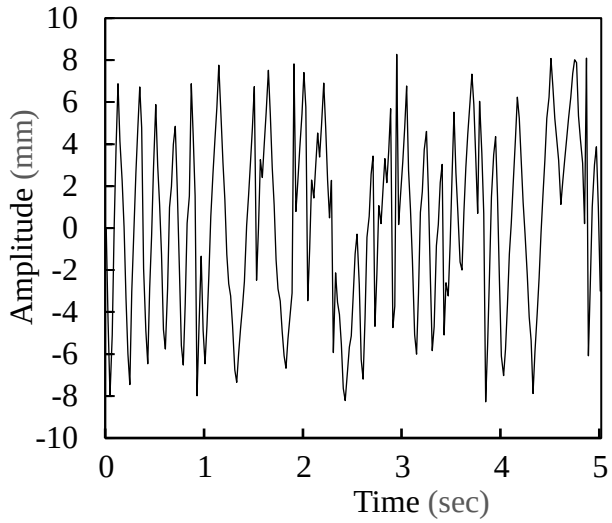

(c)

Figure A.1 Data of optimal point by using the dorsal 120° cylinder as a bluff body; (a) Stroboscopic image, (b) Normalized frequency, (c) Tail history of leading edge of the eel

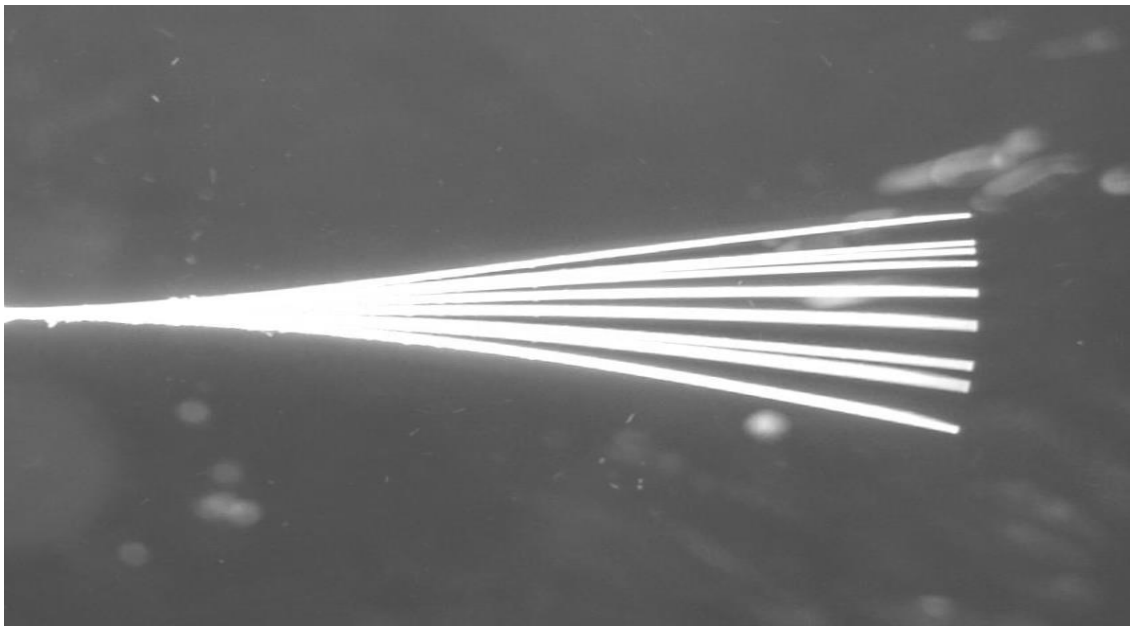

(a)

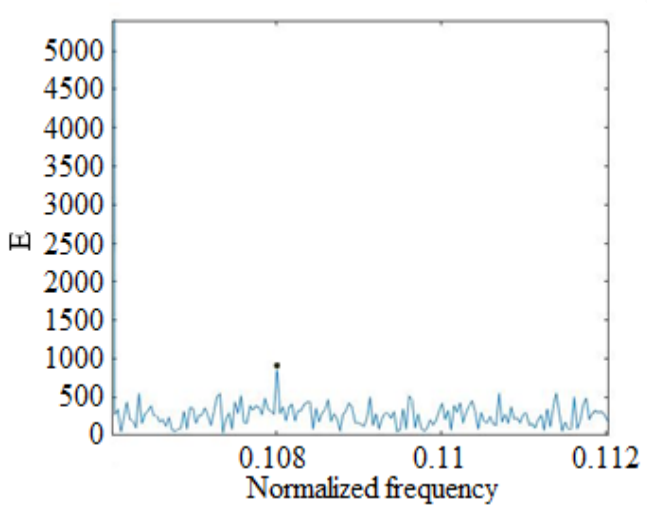

(b)

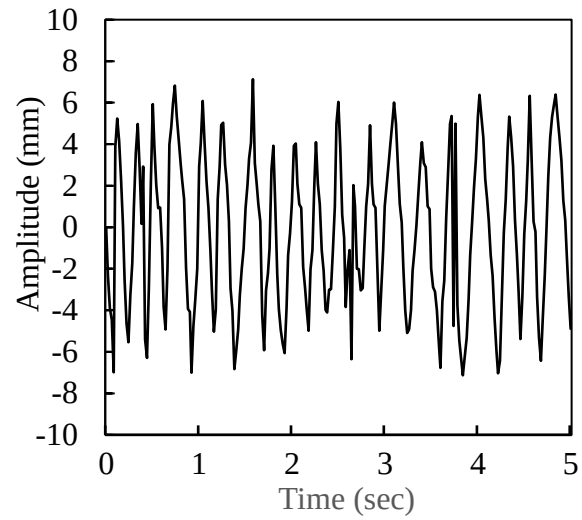

(c)

Figure A.2 Data of optimal point by using the dorsal 150° cylinder as a bluff body; (a) Stroboscopic image, (b) Normalized frequency, (c) Tail history of leading edge of the eel

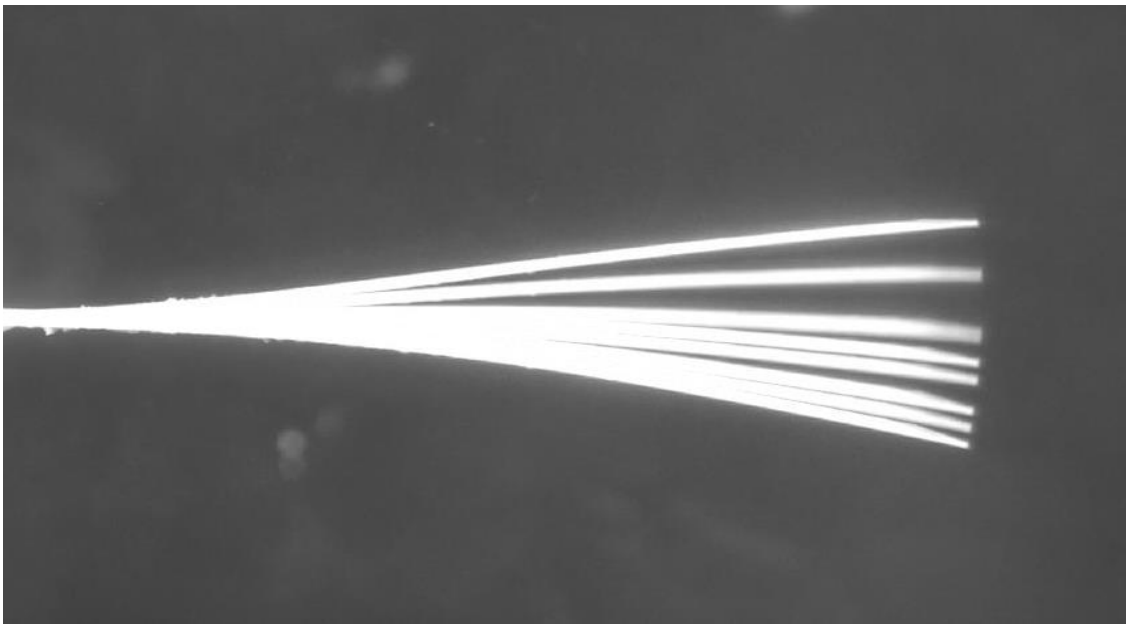

(a)

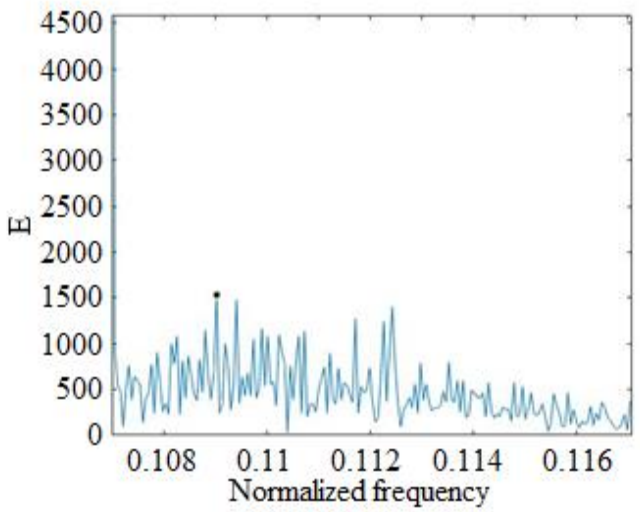

(b)

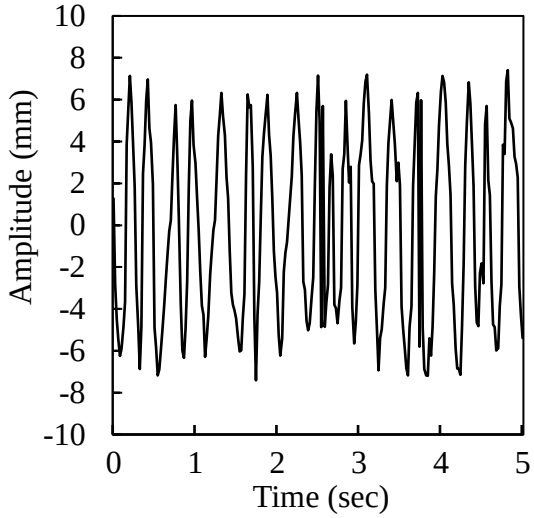

(c)

Figure A.3 Data of optimal point by using the dorsal 180° cylinder as a bluff body; (a) Stroboscopic image, (b) Normalized frequency, (c) Tail history of leading edge of the eel

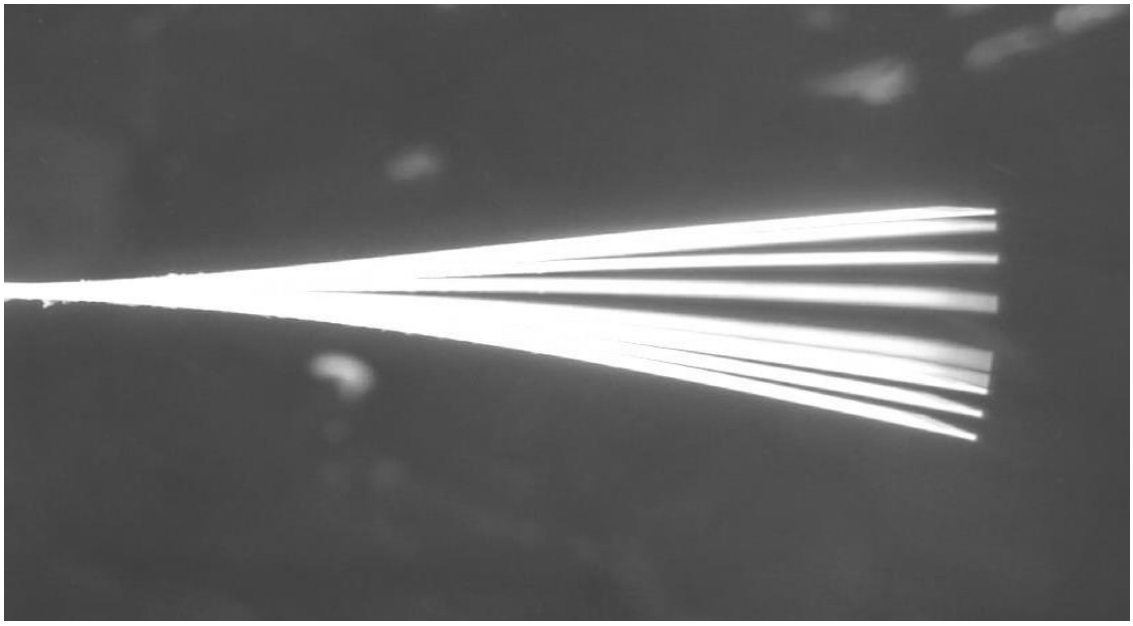

(a)

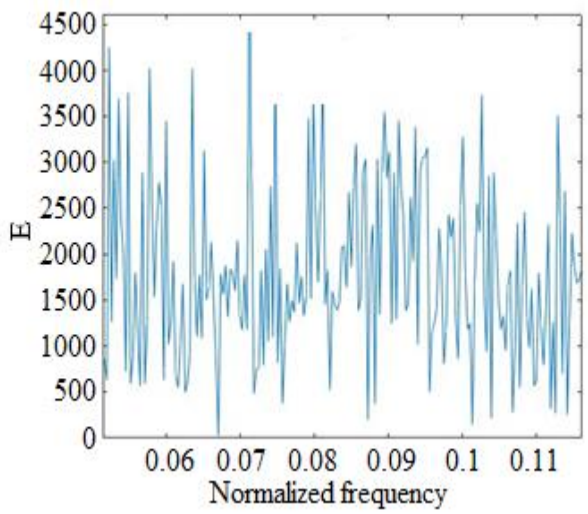

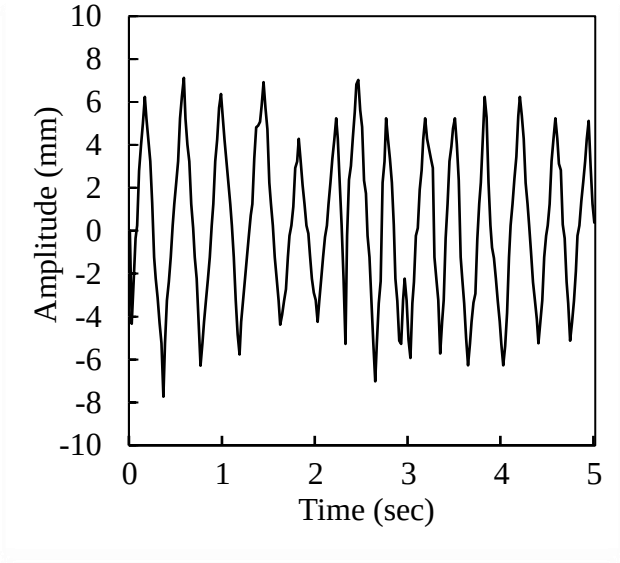

(b) (c)

Figure A.4 Data of optimal point by using the pectoral 120° cylinder as a bluff body; (a) Stroboscopic image, (b) Normalized frequency, (c) Tail history of leading edge of the eel

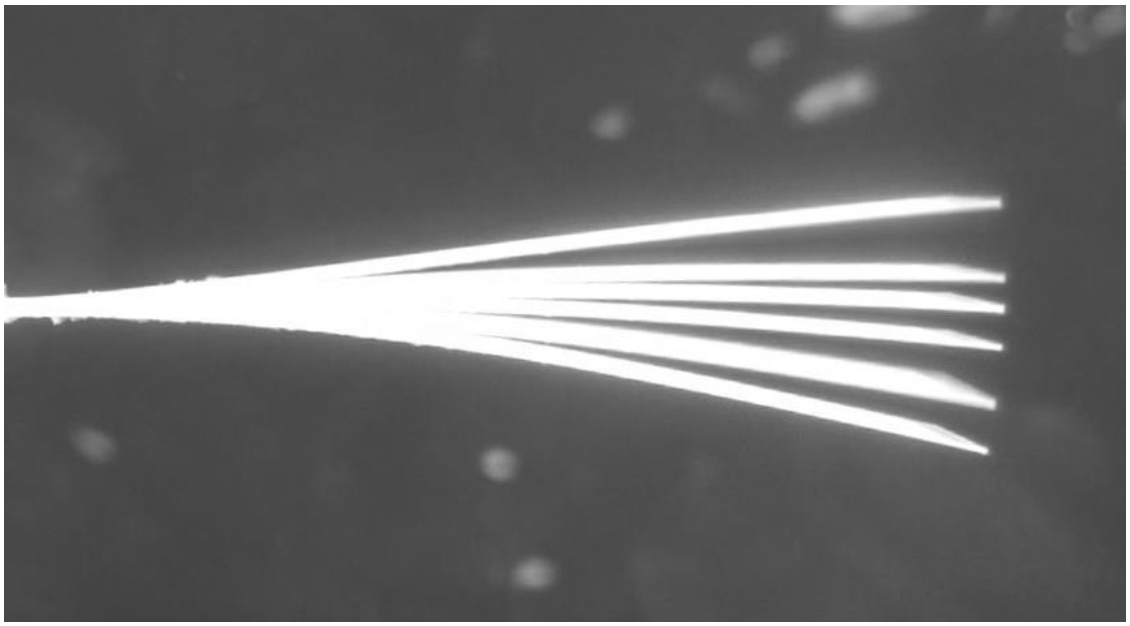

(a)

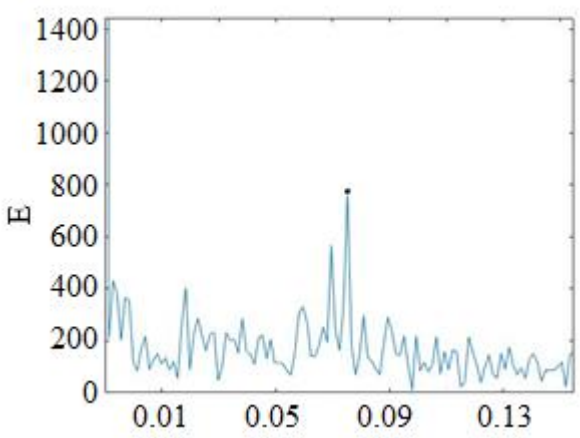

(b)

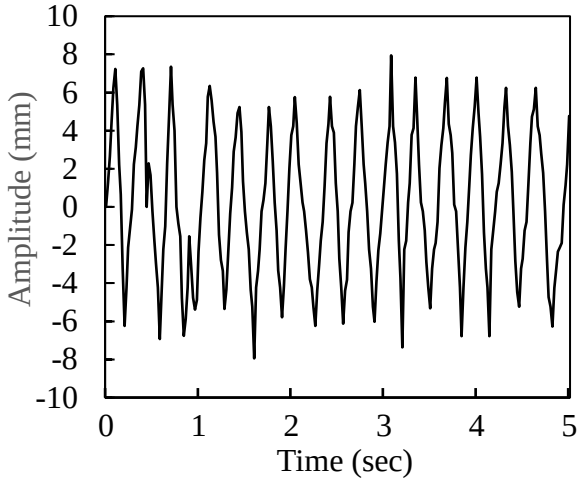

(c)

Figure A.5 Data of optimal point by using the pectoral 150° cylinder as a bluff body; (a) Stroboscopic image, (b) Normalized frequency, (c) Tail history of leading edge of the eel

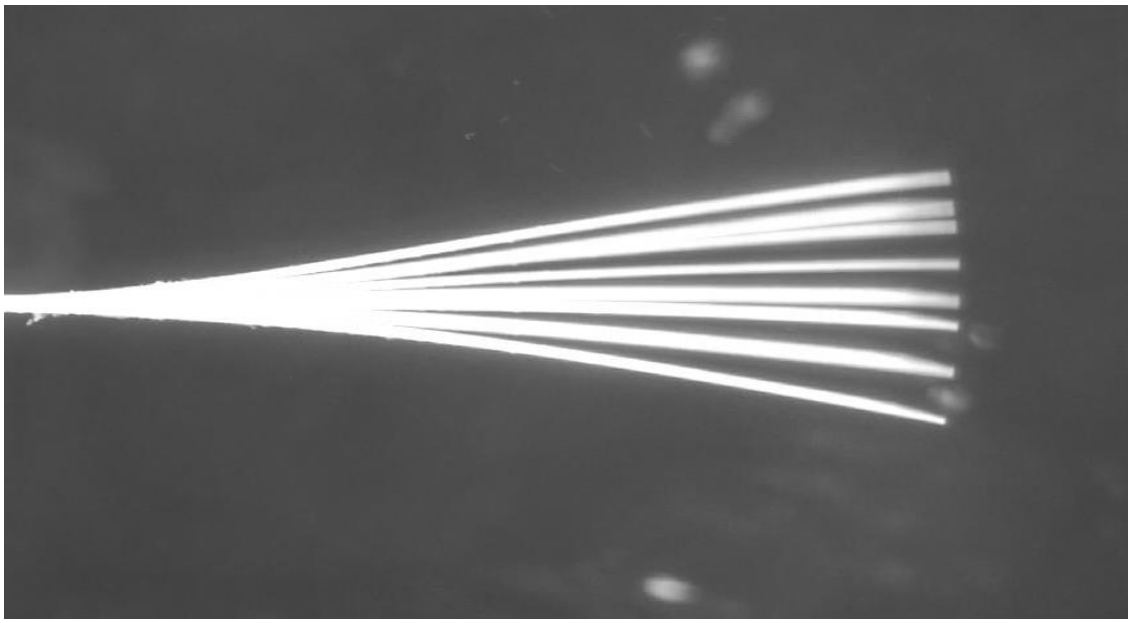

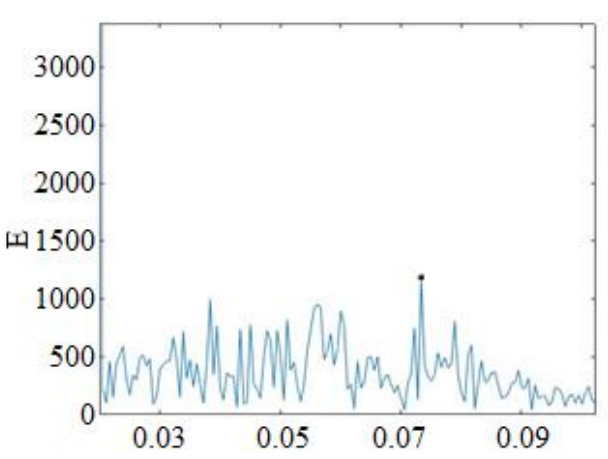

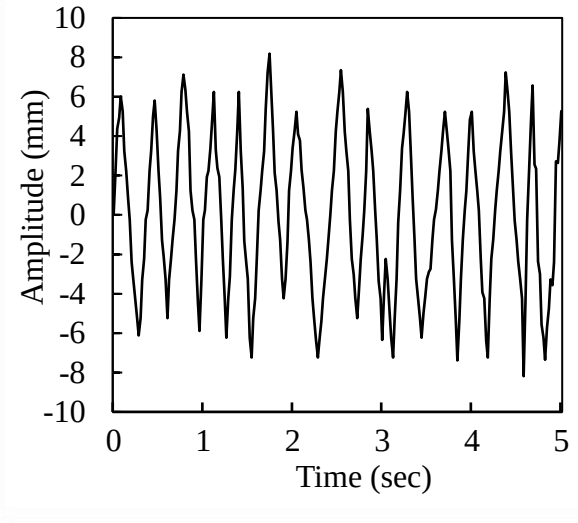

(b) (c)

Figure A.6 Data of optimal point by using the pectoral 180° cylinder as a bluff body; (a) Stroboscopic image, (b) Normalized frequency, (c) Tail history of leading edge of the eel

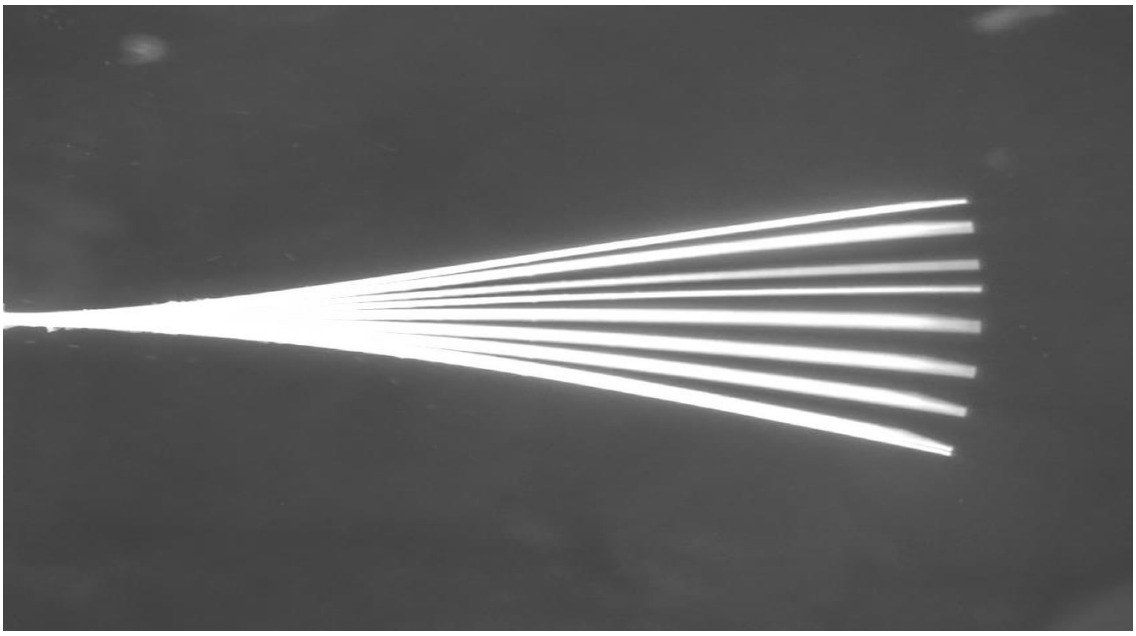

(a)

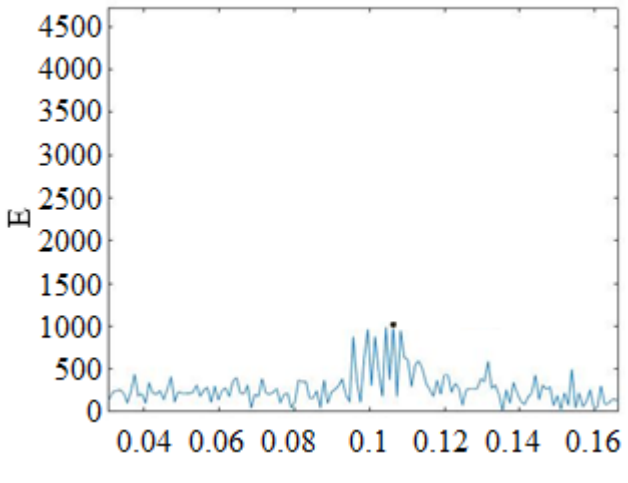

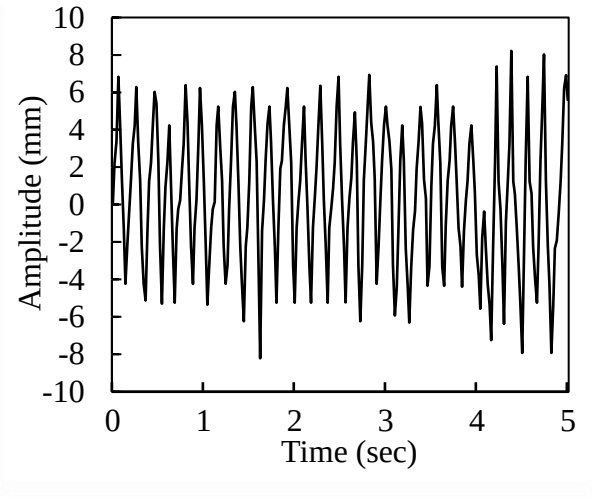

(b) (c)

Figure A.7 Data of optimal point by using the pelvic 120° cylinder as a bluff body; (a) Stroboscopic image, (b) Normalized frequency, (c) Tail history of leading edge of the eel

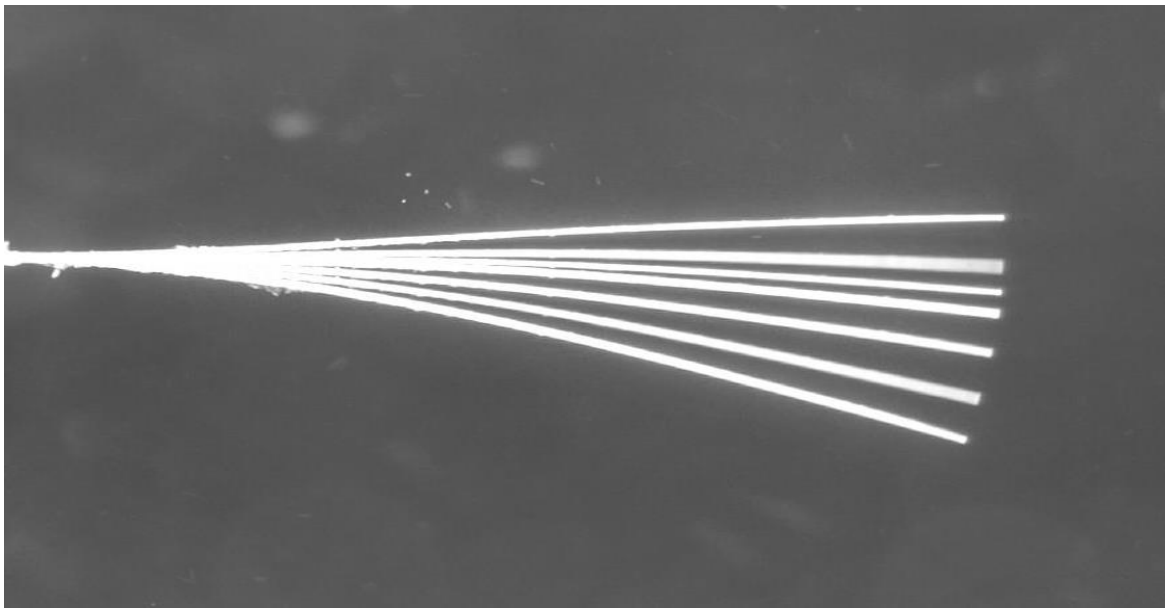

(a)

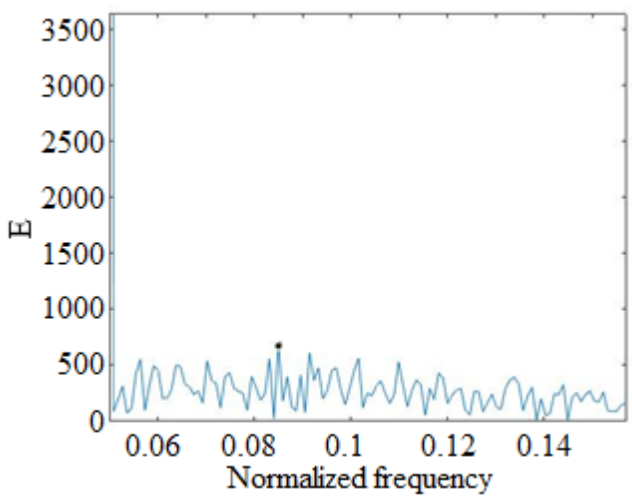

(b)

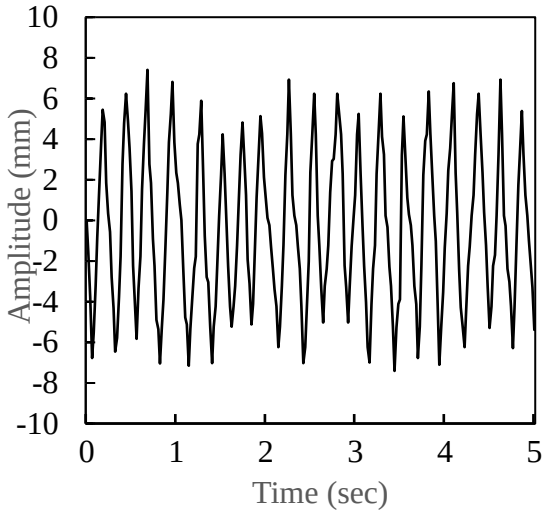

(c)

Figure A.8 Data of optimal point by using the pelvic 150° cylinder as a bluff body; (a) Stroboscopic image, (b) Normalized frequency, (c) Tail history of leading edge of the eel

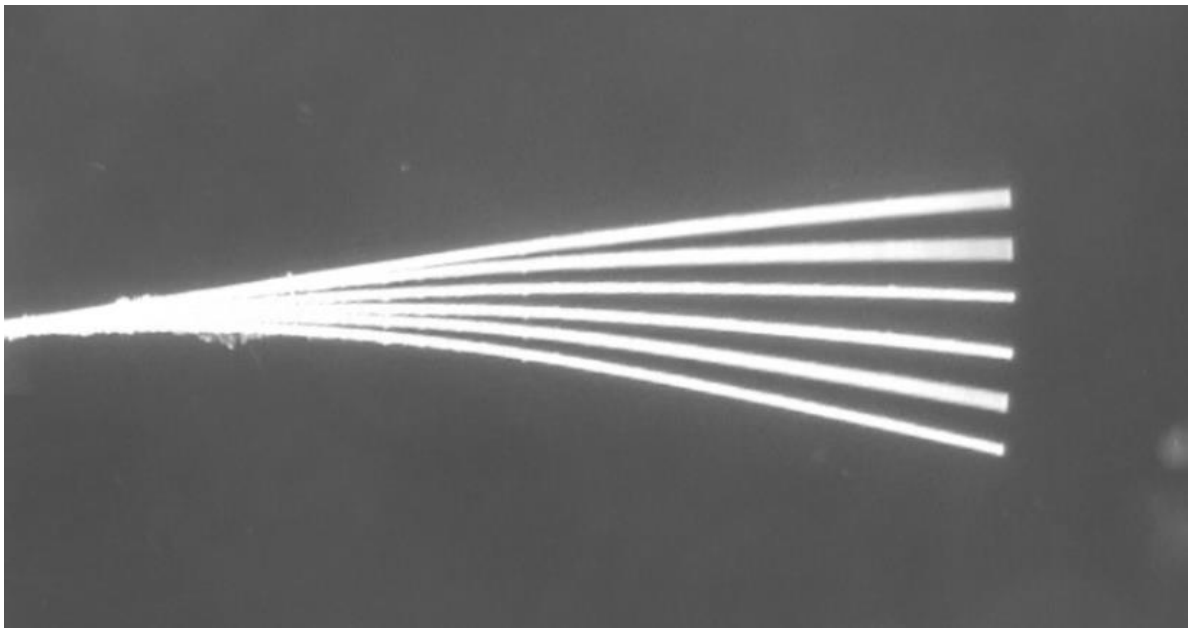

(a)

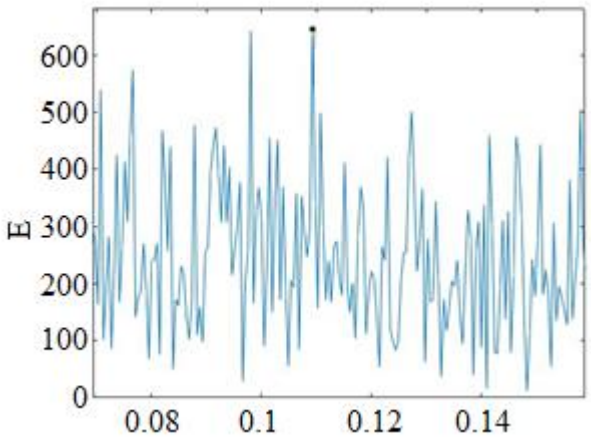

(b)

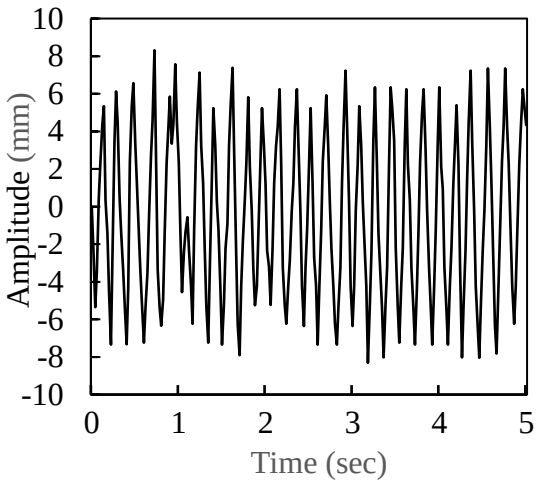

(c)

Figure A.9 Data of optimal point by using the pelvic 180° cylinder as a bluff body; (a) Stroboscopic image, (b) Normalized frequency, (c) Tail history of leading edge of the eel

Appendix – B

MATLAB Code-1

```
clc;
clear ;
close all;
% Batch Processing
video_files = {'C0004.MP4'};
vidObj = VideoReader(video_files{1}); %
I = readFrame(vidObj);
[J, rect] = imcrop(I);   % J is image and rect is coor

% Batch End

%Converting Vedio to a Array of Vector Frames
for vid = 1:length(video_files)
disp('Working on video')
vidObj = VideoReader(video_files{vid});

tip_pos = zeros(1,2);
cuurentframe = 1;

ss = zeros(size(J));   % For adding Images


vidObj.CurrentTime = 0.0;
while hasFrame(vidObj)
    F = readFrame(vidObj);
    fprintf('Current Processing Frame:\t %d\n', cuurentframe)


%Converting from RGB to Grayscale and save them in Cell Array

    U = rgb2gray(F);


%Cropping frames to desire Workspace

    Q=imcrop(U, rect); %XY value to crop them in a desired workspace




% Converting Array of Crop Images into Binary Image
     W=Q>235; %threshold to remove unwanted region
    %W = imbinarize(Q);

% Image Dilation
     %se = strel('line',100,0);  % 50 is length of line
     %gg = imdilate(W,se);
     %se = strel('line',105,0);  % 50 is length of line
```

```
     %Wm = imerode(gg,se);



    ss=ss+W;

   %---------------------

   regionstats = regionprops(W, 'all');
   [~, largestidx] = max([regionstats.Area]); %find index of largest
region

   %x=regionstats(largestidx).BoundingBox;    %coordinate of bounding box
of largest region
   %y=regionstats(largestidx).PixelList;      %coordinate of all pixels in
the region as a matrix
    h=regionstats(largestidx).Extrema;        %coordinate of extreme axis
    pcoor = (h(3,:) + h(4,:)).*0.5;
    tip_pos(cuurentframe,:) = pcoor;
    cuurentframe  = cuurentframe + 1;
%     figure; imshow(Q)
% %     figure; imshow(Wm)
%     viscircles(pcoor,10);
%     pause;
%     close;close;


end
disp('Done')
xlswrite( strcat(video_files{vid} , '.xlsx'),tip_pos)
imwrite(double(ss),strcat (video_files{vid}, '.jpg'))

end  % batch loop end
S=double(ss);
imshow(S);

% rectangle('Position',regionstats(largestidx).BoundingBox, 'EdgeColor',
% 'r') %Rectangle to check if flap is detected properly
% imshow(W)
% viscircles(pcoor,10)  TO plot a circle
[temp,originalpos] = sort( h(:,1), 'descend' );
max_num = input('Ist ? max. values to read :');
n = temp(1:max_num); % ist three max values
p=originalpos(1:max_num); % idx in original array
% [v,idx] = max(h);
val = h(p,2);
fprintf('ist three max values in ist col:\n');disp(n);
fprintf('Corresponding Values in 2nd col:\n');disp(val);


for aa =[1, 2, 3]
    disp(aa)
end
```

MATLAB Code-2

```
%% filtering matlab
clc
clear all
[v] = xlsread('C0016.MP4.xlsx', 'sheet1','D1:D3240');
dt= xlsread('C0016.MP4.xlsx', 'sheet1','C1:C3240');
figure(1)
plot(dt,v)
title ('')
xlabel('Time Step')
ylabel('Amplitude')
%% reading of excel file for specified column/values of peak and lower
position of flapping
 data = [v];
A = data'
a = max(A);
b = min(A);
c = [a,b];
xlswrite('Delta-Y.xlsx',c);
%% plot magnitude spectrum of a signal
clc
X_mags=abs(fft(v))
figure(2)
plot(X_mags)
xlabel('DFT Bins')
ylabel('Magnitude')
%% filter
%plot the first half of normalized frequency
%num_bins = length(X_mags);
num_bins = length(X_mags);
figure(3)
plot ([0:1/(num_bins/2 -1):1] , X_mags(1:num_bins/2))
xlabel('Normalizedd frequency ')  %(\pi rads/sample)
ylabel('E')
%% reading of excel file for specified column/values of voltages
 data = X_mags;
B = data'
C =(B(1,5:end))
d = max(C);
e = min(C);
f = [d,e];
xlswrite('Energy Spectra.xlsx',f);
[b_cheby,a_cheby] = cheby1(9, 0.9, 0.02, 'low');
H_cheby = freqz(b_cheby, a_cheby);
%plot filter
norm_freq_axis = [0:1/(512 -1):1];
figure(4)
plot(norm_freq_axis, abs(H_cheby),'r')
legend('Chebyshev')
xlabel('Normalised Frequency');
ylabel('Magnitude')
```

MATLAB Code-3

```
clc
clear all
close all
I = imread('C0011.MP4.jpg');
imshow(I)
```

Appendix – C

Data by using dorsal fin

Cylinder Cut angle	Gx	Gy	A/L	FF	P(μW)
120°	1.0	0.5	0.262	0.10815	82.5680
	1.5	0.5	0.267	0.10806	84.7456
	2.0	0.5	0.253	0.10400	78.7540
	2.5	0.5	0.250	0.09000	73.5670
	1.0	1.0	0.239	0.08600	69.7456
	1.5	1.0	0.232	0.07762	59.4245
	2.0	1.0	0.196	0.06793	47.6446
	2.5	1.0	0.190	0.06702	45.6560
	1.0	1.5	0.100	0.05346	35.7546
	1.5	1.5	0.138	0.05425	30.4986
	2.0	1.5	0.112	0.05386	29.4748
	2.5	1.5	0.107	0.05507	29.4960
150°	1.0	0.5	0.201	0.08500	65.3456
	1.5	0.5	0.230	0.10800	83.3940
	2.0	0.5	0.229	0.09800	76.8740
	2.5	0.5	0.186	0.07500	49.5467
	1.0	1.0	0.160	0.06300	51.4560
	1.5	1.0	0.150	0.06000	46.7345
	2.0	1.0	0.120	0.05800	52.3456
	2.5	1.0	0.110	0.05400	40.3456
	1.0	1.5	0.075	0.05000	28.4567
	1.5	1.5	0.103	0.04300	26.5070
	2.0	1.5	0.106	0.04500	27.3456
	2.5	1.5	0.097	0.04853	30.4560
180°	1.0	0.5	0.206	0.09000	70.6787
	1.5	0.5	0.224	0.09200	82.3456
	2.0	0.5	0.239	0.10700	84.8765
	2.5	0.5	0.235	0.10900	83.3456
	1.0	1.0	0.185	0.07600	54.7654
	1.5	1.0	0.180	0.07400	56.3567
	2.0	1.0	0.178	0.07300	58.3456
	2.5	1.0	0.188	0.05599	54.2345
	1.0	1.5	0.083	0.04044	24.2345
	1.5	1.5	0.065	0.03800	19.2345
	2.0	1.5	0.068	0.03400	17.7654
	2.5	1.5	0.111	0.03300	25.76543

Table C.1 Data by using dorsal fin with different cut angle cylinders as a bluff body

Data by using pectoral fin

Cylinder Cut angle	Gx	Gy	A/L	FF	P(μW)
120°	1.0	0.5	0.164	0.06136	62.5678
	1.5	0.5	0.156	0.06447	56.4563
	2.0	0.5	0.143	0.05725	54.9346
	2.5	0.5	0.154	0.05274	43.6543
	1.0	1.0	0.237	0.07254	67.9877
	1.5	1.0	0.220	0.06926	66.3457
	2.0	1.0	0.138	0.05963	56.3457
	2.5	1.0	0.146	0.05852	41.9543
	1.0	1.5	0.102	0.05963	34.5420
	1.5	1.5	0.101	0.05763	33.5432
	2.0	1.5	0.102	0.05893	31.6543
	2.5	1.5	0.102	0.05163	29.6543
150°	1.0	0.5	0.175	0.06247	60.3456
	1.5	0.5	0.185	0.05635	58.6543
	2.0	0.5	0.175	0.05736	53.6543
	2.5	0.5	0.164	0.05530	54.6543
	1.0	1.0	0.256	0.07436	69.7654
	1.5	1.0	0.234	0.05753	65.6430
	2.0	1.0	0.225	0.05636	60.6543
	2.5	1.0	0.206	0.05613	58.8765
	1.0	1.5	0.114	0.05737	37.3543
	1.5	1.5	0.102	0.03459	22.7654
	2.0	1.5	0.186	0.05973	54.7645
	2.5	1.5	0.222	0.05529	58.4569
180°	1.0	0.5	0.264	0.07356	56.2345
	1.5	0.5	0.262	0.07234	54.6345
	2.0	0.5	0.262	0.06141	55.7654
	2.5	0.5	0.256	0.06282	58.4567
	1.0	1.0	0.089	0.06502	33.2346
	1.5	1.0	0.104	0.06501	36.5435
	2.0	1.0	0.118	0.06348	39.3465
	2.5	1.0	0.141	0.06592	47.3458
	1.0	1.5	0.187	0.06225	57.3458
	1.5	1.5	0.195	0.06357	58.3477
	2.0	1.5	0.219	0.06406	60.7653
	2.5	1.5	0.205	0.06296	55.2348

Table C.2 Data by using pectoral fin with different cut angle cylinders as a bluff body

Data by using pelvic fin

Cylinder Cut angle	Gx	Gy	A/L	FF	P(μW)
120°	1.0	0.5	0.265	0.10700	82.5790
	1.5	0.5	0.261	0.10800	83.7200
	2.0	0.5	0.243	0.09200	56.4990
	2.5	0.5	0.228	0.08300	54.6435
	1.0	1.0	0.211	0.06600	53.9346
	1.5	1.0	0.210	0.06800	50.7654
	2.0	1.0	0.187	0.06793	48.7653
	2.5	1.0	0.178	0.05400	49.2346
	1.0	1.5	0.110	0.03800	28.6512
	1.5	1.5	0.129	0.03200	25.6512
	2.0	1.5	0.106	0.03500	23.5321
	2.5	1.5	0.127	0.03700	21.2346
150°	1.0	0.5	0.185	0.07890	39.3450
	1.5	0.5	0.239	0.08500	71.1690
	2.0	0.5	0.178	0.08200	65.6270
	2.5	0.5	0.185	0.06300	45.2520
	1.0	1.0	0.173	0.05800	47.3457
	1.5	1.0	0.181	0.06400	50.8765
	2.0	1.0	0.179	0.05900	48.4568
	2.5	1.0	0.177	0.06700	52.4570
	1.0	1.5	0.181	0.04700	32.6535
	1.5	1.5	0.175	0.03800	29.0457
	2.0	1.5	0.178	0.03500	26.2346
	2.5	1.5	0.189	0.03230	27.3457
180°	1.0	0.5	0.194	0.08400	61.8765
	1.5	0.5	0.218	0.07600	65.3457
	2.0	0.5	0.258	0.09900	79.4568
	2.5	0.5	0.268	0.10900	83.3457
	1.0	1.0	0.192	0.06800	44.4570
	1.5	1.0	0.163	0.06200	43.4590
	2.0	1.0	0.158	0.05400	47.3710
	2.5	1.0	0.145	0.04700	49.1640
	1.0	1.5	0.102	0.03800	28.4568
	1.5	1.5	0.085	0.04200	24.8764
	2.0	1.5	0.074	0.03500	22.7635
	2.5	1.5	0.069	0.03700	19.3459

Table C.3 Data by using pelvic fin with different cut angle cylinders as a bluff body